THESIS FOR THE DEGREE OF LICENTIATE OF ENGINEERING IN THERMO AND FLUID DYNAMICS

Numerical Modeling of Atomization in Spray Systems

MICHELE PÜTZ

Department of Mechanics and Maritime Sciences,
Division of Combustion and Propulsion Systems

CHALMERS UNIVERSITY OF TECHNOLOGY

Gothenburg, Sweden 2019

Numerical Modeling of Atomization in Spray Systems
MICHELE PÜTZ

Thesis for the degree of Licentiate of Engineering 2019:02
Department of Mechanics and Maritime Sciences,
Division of Combustion and Propulsion Systems
Chalmers University of Technology
SE-412 96 Gothenburg
Sweden
Telephone: +46 (0)31-772 1000

Chalmers Reproservice
Gothenburg, Sweden 2019

Numerical Modeling of Atomization in Spray Systems
Thesis for the degree of Licentiate of Engineering in Thermo and Fluid Dynamics
MICHELE PÜTZ
Department of Mechanics and Maritime Sciences,
Division of Combustion and Propulsion Systems
Chalmers University of Technology

Abstract

Dispersed multiphase flows refer to dynamic systems comprising two or more phases where at least one phase is in the form of fine particles evolving in and interacting with a surrounding fluid. Spray systems fall into that category. Several technical applications highlight the significance of sprays, one of which is the injection of liquid fuel in propulsion systems, where the spray formation, vaporization and subsequent mixing prior to combusion determine fuel efficiency and the emission of pollutants that are hazardous to human health and nature. Optimization of such systems requires the understanding of spray physics. While theoretical analysis and experiments remain essential methods with regard to the optimization of such systems, the advance in computer performance over the past few decades has made numerical simulation an additional powerful tool to improve spray systems. However, the existence of physical and predictive models is crucial. This thesis is concerned with the physical phenomena that are present in spray systems and the transfer to suitable computational models. In terms of spray physics, the focus is on atomization which refers to the disintegration of liquid structures. Another central aspect of spray modeling is the representation of the particulate phase. The numerical models studied as part of this work are the one-dimensional turbulence model for the breakup of a liquid jet combined with standard Lagrangian methods as well as a family of Eulerian population balance models, the so-called quadrature-based moment methods. Numerical investigations were carried out on a gasoline spray as well as less complex configurations and give many suggestions for future research.

Keywords: Multiphase, atomization, spray modeling, numerical simulation, population balance equations, quadrature-based moment methods

List of publications

This thesis is partially based on the work contained in the following publications:

Publication I M. Pütz, A. Movaghar and M. Oevermann. "Numerical Simulation of a Gasoline Spray Using One-Dimensional Turbulence for Primary Atomization". *ICLASS 2018, 14 th Triennial International Conference on Liquid Atomization and Spray Systems, Chicago, IL, USA, July 22-26, 2018*. 2018.

Acknowledgements

As there are some people that deserve to be acknowledged, this page shall not remain blank. First and foremost, I would like to thank my supervisor Michael Oevermann for giving me the freedom to pursue my own ideas and always being helpful when I seek advice. His way of supervision creates the best imaginable working conditions for me and keeps me motivated.

Next, I want to thank Martin Pollack and Christian Hasse for their hospitality during my visits in Darmstadt and Freiberg. The many fruitful discussions during the time of our collaboration helped me remain on track and stay focused.

Moreover, I thank Ingemar Denbratt for his part in hiring me as well as his successor Lucien Koopmans for supporting my stay "abroad". I also want to express my gratitude to the Swedish energy agency for the project funding.

Also, the support of my family and friends (some more and others less) should not go unmentioned.

I offer my gratitide and sincerest apologies to everyone I should have mentioned here.

Contents

1 Introduction

Multiphase flows are common in a wide range of natural phenomena and technical applications. A few examples of their occurence in nature are - from large to small scales - weather patterns, ocean dynamics and blood flow. On the other side, propulsion systems, power generation, heat exchange and manufacturing technologies highlight the importance of multiphase flows in technical and industrial applications. If at least one phase in such a system appears in the form of fine particles, it is referred to as dispersed multiphase flow. Sprays, i.e. systems comprising liquid droplets that evolve in a surrounding gas, are an example of dispersed multiphase flows of technical importance.

In propulsion systems that rely on the combustion of hydrocarbon-based fuels as the primary source for power generation, sprays are of particular interest, as spray physics critically affect the formation and emission of pollutants as well as the efficiency. A well-known and much-debated example that highlights the relevance of sprays in technical applications is the direct injection of liquid fuel into the combustion chamber of an engine, which is nowadays the standard approach in modern engines with both spark ignition and compression ignition. The injection is followed immediately by a combination of interdependent physical processes, all of which have a significant impact on the distribution of fuel in the chamber prior to combustion and consequently on the engine efficiency as well as the formation of toxic substances that are considered harmful to human health and nature. Minimizing the negative effects of engine combustion requires the optimization of the mixture formation as an essential element in the whole chain of processes.

The physical phenomena appearing in spray systems are the internal nozzle flow, which may include a pressure-driven phase change (cavitation), the primary breakup of a liquid jet into smaller structures forming a particulate system, the secondary breakup of formed droplets into smaller droplets, and the vaporization of liquid droplets to form a gas-vapor mixture.

In order to gain understanding and improve such processes to optimize technical systems, numerical simulations have become an increasingly important tool besides experimental investigations over the past few decades, mainly owing to the rapid advance in computational performance. However, predictive simulations of sprays or dispersed multiphase flows in general require the understanding of the above-mentioned phenomena as well as the development and implementation of models with adequate accuracy and affordable computational costs. This thesis is concerned with the numerical modeling of spray systems, in particular atomization processes and subsequent evaporation. The thesis is structured as described below.

In *Chapter 2* the fundamental equations governing dispersed multiphase systems in general are given. The main focus is on the mathematical description of the continuous phase and particulate systems that are governed by population balance equations (PBE) instead of modeling approaches that treat the dispersed particles as continuous media.

Chapter 3 covers modeling approaches of spray systems in general. The emphasis is on models that aim at the description of the dispersed phase and gas-droplet interaction. A central modeling approach described in Chapter 3 are the quadrature-based moment methods (QBMM), a family of methods that approximate solutions to PBEs in an Eulerian framework by exploiting integral properties, namely moments of local distribution functions.

Chapter 4 concentrates on liquid atomization. The essential physical phenomena causing fragmentation as well as models for primary and secondary atomization are presented and discussed. A particular focus is placed on the one-dimensional turbulence model in conjunction with a Lagrangian representation of the particulate phase, as well as the modeling of secondary droplet breakup with QBMM.

Chapter 5 contains some results of numerical studies, namely simulations of a gasoline spray applying different models as well as less complex test cases for the validation of QBMM. The latter is focused on the investigation of isolated physical phenomena as a step towards spray simulations with QBMM.

Chapter 6 summarizes the thesis with some concluding remarks and suggestions for future research to advance numerical methods for spray systems.

2 Mathematical Description of Dispersed Multiphase Systems

This chapter provides a brief introduction to the mathematical description of dispersed multiphase flows. First however, a few notes on the terminology used here are necessary. The term "dispersed multiphase system" describes a system of at least two phases, where one phase, that can be a gas, liquid or solid, is present in a dispersed form, i.e. in form of small particles with a small total volume fraction. The focus of the present thesis is on two-phase systems. The dispersed phase is also referred to as dispersed system or particulate phase/system. The other phase that occupies most of the volume is called the continuous phase as it is treated as continuous matter. Whereas considerations in later sections are presented with a focus on sprays, i.e. a large number of small liquid droplets dispersed in gas, the mathematical descriptions given in this section are rather general and can be applied to multiphase flows involving particles of any state of matter. For convenience, the following descriptions will relate to two-phase flows, although extension to more than two phases is possible in most cases.

A variety of modeling approaches exists for dispersed multiphase flows. However, they can generally be divided into two classes: (1) Interface-resolving methods and (2) population balance models. Interface-resolving methods treat both phases as continuous fluids with mass, momentum and energy transfer across the interface. Common examples are interface-tracking/capturing methods such as level-set [60] and volume-of-fluid [33] methods as well as the so-called two-fluid methods, where the phases are treated as interpenetrating continua and two sets of field equations are solved. Since such approaches generally require a high numerical resolution in space and time to be able to resolve interfaces on the computational grid, they are often combined with large-eddy simulation (LES) or direct numerical simulations (DNS). Interface-resolving techniques provide a high degree of accuracy but are numerically expensive and therefore unfeasible for the simulation of many technical problems.

The second class of multiphase models are the population balance models. Instead of the representation of each phase as a continuum, the dispersed phase is modeled on a population scale, not on a particle scale. In other words, the main interest is not a detailed understanding of the processes at the interfaces or properties of single entities of the population, but a statistical description of the particulate system, of which the evolution is governed by a population balance equation (PBE). The focus of this thesis is placed on population balance models.

This chapter is structured as follows. First, the different specifications of a fluid mechanical system in a Lagrangian and an Eulerian frame of reference and the transformation between those two approaches by means of the Reynolds transport theorem are introduced. Based on that, the Eulerian fundamental governing equations of non-isothermal flows are derived. Following this, different forms of the PBE are given in order to provide the

foundation for later considerations in the context of dispersed multiphase flows. The chapter concludes with the definition of dimensionless quantities that are characteristic for dispersed multiphase flows.

2.1 Fundamental Equations in Fluid Mechanics - Lagrangian and Eulerian Representation

The governing conservation equations for the flow of continuous media are all specific forms of the same type of equation. This section gives a brief derivation of a general Eulerian transport equation, which provides the basis for the conservation equations presented in the following sections. For more elaborate derivations the reader is referred to the abundant literature on this topic, e.g. [5, 22, 92].

The rate of change of an arbitrary scalar or vectorial variable Φ of a fluid element traveling in an N-dimensional space is described by its total derivative with respect to time t and the spatial coordinates x_i:

$$\frac{D\Phi}{Dt} = \frac{\partial \Phi}{\partial t} + \sum_{i=1}^{N} \frac{\partial \Phi}{\partial x_i} \frac{\partial x_i}{\partial t} \,. \tag{2.1}$$

By convention, the term $D\Phi/Dt$ denotes the so-called material derivative or substantial derivative. As $\partial\Phi/\partial x_i$ corresponds to the velocity component in ith direction u_i, it can be expressed as

$$\frac{D\Phi}{Dt} = \frac{\partial \Phi}{\partial t} + \sum_{i=1}^{N} u_i \frac{\partial \Phi}{\partial x_i} \tag{2.2}$$

or in vector notation

$$\frac{D\Phi}{Dt} = \frac{\partial \Phi}{\partial t} + \mathbf{u} \bullet \boldsymbol{\nabla} \Phi, \tag{2.3}$$

where $\boldsymbol{\nabla} = [\partial/\partial x_1, \quad \partial/\partial x_2, \quad \ldots, \quad \partial/\partial x_n]^{\mathrm{T}}$ is the vector differential operator with respect to $\mathbf{x}$. Eq. 2.3 describes the evolution of a material element, i.e. a moving control volume/mass. This is also called the Lagrangian specification of a system, and accordingly $D\Phi/Dt$ is also referred to as the Lagrangian derivative of Φ. However, since we are usually not interested in the evolution of material elements but rather in the local change of a field within a specific domain, this type of description is not practical in terms of numerical simulations. Instead, an Eulerian specification of the system, i.e. a specifiction in terms of fixed control volumes, is desired in most cases. The difference between the Lagrangian and the Eulerian approach is illustrated in Figure 2.1.

Laws of mechanics such as the laws of mass and momentum conservation are formulated for a system, which is in this case defined as an arbitrary quantity of matter. Thus, the

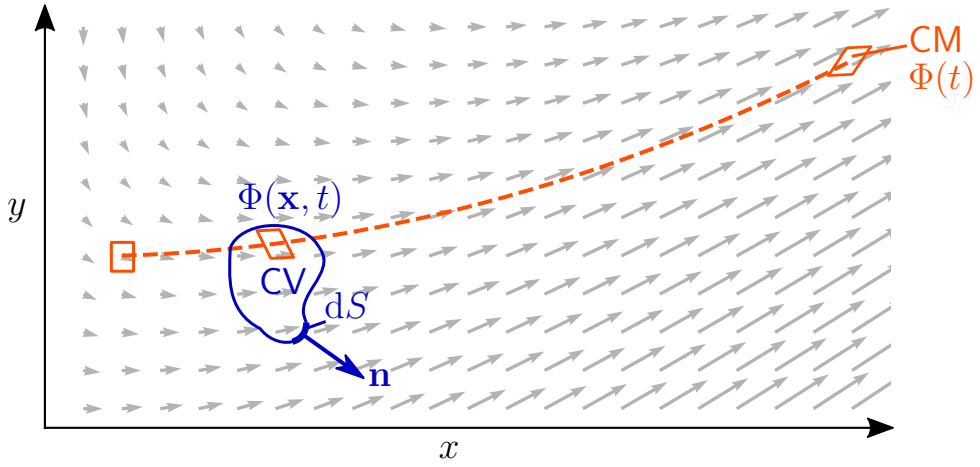

Figure 2.1: *Illustration of the difference between an Eulerian and a Lagrangian description using the example of a two-dimensional flow field. The Eulerian specification (blue) is based on a control volume (CV) that is independent of the flow field and not associated with a particular mass. In the Lagrangian description (orange), a moving control mass (CM) specified as an arbitrary amount of substance with fixed identity is the observed system, which is also deformed here. The dashed line is the streamline/pathline associated with the depicted control mass.*

formulation corresponds to the Lagrangian description. An equivalent Eulerian description of a fluid system is obtained by applying Reynolds' theorem

$$\left(\frac{\mathrm{d}\Phi}{\mathrm{d}t}\right)_{sys} = \frac{\mathrm{d}}{\mathrm{d}t}\left(\int_V \phi\rho\,\mathrm{d}V\right) + \oint_S \phi\rho\,(\mathbf{u}-\mathbf{u_s})\bullet\mathbf{n}\,\mathrm{d}S, \tag{2.4}$$

where $\phi = \Phi/m$ is the intensive property related to the extensive property Φ, V is a fixed control volume with the boundary S, $\mathbf{u_s}$ is the velocity of the control surface and $\mathbf{n}$ is the unit normal vector as depicted in Figure 2.1. Applying Leibniz's integral rule,

$$\frac{\mathrm{d}}{\mathrm{d}t}\int_V f\,\mathrm{d}V = \int_V \frac{\partial f}{\partial t}\,\mathrm{d}V + \oint_S \mathbf{n}\bullet\mathbf{u}_s\mathbf{f}\,\mathrm{d}S \tag{2.5}$$

and presuming a fixed, time-invariant, non-deformable control volume, i.e. $\mathbf{u_s} = \mathbf{0}$, Eq. 2.4 can be written as

$$\left(\frac{\mathrm{d}\Phi}{\mathrm{d}t}\right)_{sys} = \int_V \frac{\partial}{\partial t}\,\phi\rho\,\mathrm{d}V + \oint_S \phi\rho\mathbf{u}\bullet\mathbf{n}\,\mathrm{d}S. \tag{2.6}$$

Applying Gauss' divergence theorem

$$\int_V \boldsymbol{\nabla}\bullet\mathbf{f}\,\mathrm{d}V = \oint_S \mathbf{n}\bullet\mathbf{f}\,\mathrm{d}S, \tag{2.7}$$

the surface integral in Eq. 2.6 can be transformed into a volume integral and the rate of change finally reads

$$\left(\frac{\mathrm{d}\Phi}{\mathrm{d}t}\right)_{sys} = \int_V \left[\frac{\partial}{\partial t}\,\phi\rho + \boldsymbol{\nabla}\bullet(\rho\mathbf{u}\phi)\right]\mathrm{d}V. \tag{2.8}$$

By substituting the dummy field variable Φ with quantities that obey laws of continuum mechanics and thermodynamics with respect to a mass of fixed identity (Lagrangian), the Eulerian field transport equations can be derived, which will be done in the following section, with Eq. 2.8 serving as the basis.

2.2 The Continuous Phase

2.2.1 Transport Equations

2.2.1.1 The Continuity Equation

The principle of conservation of mass states that the mass in a closed system is constant, i.e. $(\mathrm{d}m/\,\mathrm{d}t)_{sys} = 0$. However, in dispersed multiphase systems or multiphase systems in general, the exchange of mass between the phases has to be accounted for. Applying Eq. 2.8 to mass, i.e. $\Phi = m, \phi = 1$ and introducing a source term per unit volume $\mathcal{Q}_\rho$ accounting for mass transfer between the continuous and the dispersed phase, we can write

$$\int_V \left(\frac{\partial\rho}{\partial t} + \boldsymbol{\nabla}\bullet(\mathbf{u}\rho) - \mathcal{Q}_\rho\right)\mathrm{d}V = 0 \tag{2.9}$$

For an arbitrary control volume V, Eq. 2.9 is satisfied if the integrand is zero. Thus, the differential equation for mass conservation reads

$$\frac{\partial\rho}{\partial t} + \boldsymbol{\nabla}\bullet(\mathbf{u}\rho) = \mathcal{Q}_\rho. \tag{2.10}$$

2.2.1.2 The Species Equation

In flows involving multiple species, the conservation of mass can be written as a species transport equation. This is necessary for sprays, where spatial mixture inhomogeneities due to evaporation are of interest. In a system that involves N species, the transport of the ith species is governed by

$$\frac{\partial}{\partial t}(\rho Y_i) + \boldsymbol{\nabla}\bullet(\rho\mathbf{u}Y_i) - \boldsymbol{\nabla}\bullet(\rho\mathcal{D}_i\boldsymbol{\nabla}Y_i) = \mathcal{Q}_{Y_i}, \tag{2.11}$$

where $Y_i = m_i/m$ and $\mathcal{D}_i$ are the mass fraction and mass diffusivity of the ith species, respectively. It is important to note that - in contrast to the total mass - diffusive fluxes

of species across the system boundaries can take place. Naturally, since Y_i are defined as mass fractions

$$\sum_{i=1}^{N} Y_i = 1. \tag{2.12}$$

Eq. 2.10, 2.11 and 2.12 constitute an over-determined, albeit physically consistent system of equations. However, solving it numerically, the species diffusion term potentially causes a violation of Eq. 2.12 or Eq. 2.10. A common approach to prevent that is to solve Eq. 2.11 only for $N-1$ species and enforce mass conservation by means of Eq. 2.10 and 2.12.

2.2.1.3 The Momentum Equation

A summary of the derivation of the momentum (Navier-Stokes) equation for an Eulerian specification of the system is given in this section. It is based on the references [5, 22, 56, 91, 92], which contain more in-depth explanations.

The momentum equation is derived from the conservation of linear momentum and Newton's second law

$$\mathbf{F_{tot}} = m\mathbf{a} = m\frac{\mathrm{d}\mathbf{u}}{\mathrm{d}t} \tag{2.13}$$

where $\mathbf{F_{tot}}$ is the total external force acting on the system and $\mathbf{a}$ is the vector of acceleration. For a system of constant mass this is equivalent to

$$\left(\frac{\mathrm{d}}{\mathrm{d}t}(m\mathbf{u})\right)_{sys} = \sum \mathbf{F}. \tag{2.14}$$

The forces acting on a fluid element can generally be divided into body forces, which are only the force due to gravitation here, and surface forces due to the stresses acting on the surface of a fluid parcel. Then the change of momentum of the material element is expressed as

$$\left(\frac{\mathrm{d}}{\mathrm{d}t}(m\mathbf{u})\right)_{sys} = \int_V \rho\mathbf{g}\,\mathrm{d}V + \oint_S \boldsymbol{\sigma}\bullet\mathbf{n}\,\mathrm{d}S, \tag{2.15}$$

where $\mathbf{g}$ is the gravitational acceleration vector and $\boldsymbol{\sigma}$ is the 3x3 stress tensor that can be decomposed into static pressure and viscous stresses (also referred to as hydrodynamic and deviatoric stresses, respectively):

$$\boldsymbol{\sigma} = \begin{bmatrix}\sigma_{11} & \sigma_{12} & \sigma_{13}\\ \sigma_{21} & \sigma_{22} & \sigma_{23}\\ \sigma_{31} & \sigma_{32} & \sigma_{33}\end{bmatrix} = -\begin{bmatrix}p & 0 & 0\\ 0 & p & 0\\ 0 & 0 & p\end{bmatrix} + \begin{bmatrix}\tau_{11} & \tau_{12} & \tau_{13}\\ \tau_{21} & \tau_{22} & \tau_{23}\\ \tau_{31} & \tau_{32} & \tau_{33}\end{bmatrix} = -p\mathbf{I} + \boldsymbol{\tau}, \tag{2.16}$$

where p, $\mathbf{I}$ and $\boldsymbol{\tau}$ are the static pressure, the 3x3 identity tensor and the $\boldsymbol{\tau}$ the viscous stress tensor, respectively. Using this expression as well as Gauss' divergence theorem for

the transformation of a surface integral into a volume integral (Eq. 2.7), the second term on the RHS of Eq. 2.15 can be written as

$$\oint_S \boldsymbol{\sigma} \bullet \mathbf{n} \, \mathrm{d}S = \int_V \boldsymbol{\nabla} \bullet (-p\mathbf{I} + \boldsymbol{\tau}) \, \mathrm{d}V = \int_V (-\boldsymbol{\nabla} p + \boldsymbol{\nabla} \bullet \boldsymbol{\tau}) \, \mathrm{d}V. \tag{2.17}$$

Substituting $\Phi = m\mathbf{u}$, $\phi = \mathbf{u}$, Eq. 2.15 and 2.17 into Eq.2.8 gives

$$\int_V \left(\frac{\partial}{\partial t} (\rho \mathbf{u}) + \boldsymbol{\nabla} \bullet (\rho \mathbf{u}\mathbf{u}) \right) \mathrm{d}V = \int_V (-\boldsymbol{\nabla} p + \boldsymbol{\nabla} \bullet \boldsymbol{\tau} + \rho \mathbf{g}) \, \mathrm{d}V, \tag{2.18}$$

which is satisfied for an arbitrary control volume V if

$$\frac{\partial}{\partial t} (\rho \mathbf{u}) + \boldsymbol{\nabla} \bullet (\rho \mathbf{u}\mathbf{u}) = -\boldsymbol{\nabla} p + \boldsymbol{\nabla} \bullet \boldsymbol{\tau} + \rho \mathbf{g}. \tag{2.19}$$

Eq. 2.19 is the general equation for the conservation of momentum. For Newtonian fluids, it can be written in a different form, since the viscous stress tensor can be expressed as a linear function of the strain rate, namely

$$\boldsymbol{\tau} = \mu \left[\boldsymbol{\nabla} \mathbf{u} + (\boldsymbol{\nabla} \mathbf{u})^{\mathrm{T}} \right] + \lambda (\boldsymbol{\nabla} \cdot \mathbf{u}) \mathbf{I}, \tag{2.20}$$

where μ is the dynamic viscosity and λ is the bulk viscosity, which is usually set equal to $-2/3\mu$. Introducing an additional source term $\mathcal{Q}_{\mathbf{u}}$ for the momentum transfer transfer from the dispersed phase, the momentum equation for the continuous phase of a Newtonian fluids is

$$\begin{aligned} \frac{\partial}{\partial t} (\rho \mathbf{u}) + \boldsymbol{\nabla} \bullet (\rho \mathbf{u}\mathbf{u}) = & - \boldsymbol{\nabla} p + \boldsymbol{\nabla} \bullet (\mu \boldsymbol{\nabla} \mathbf{u}) + \boldsymbol{\nabla} \bullet \left[\mu \left(\boldsymbol{\nabla} \mathbf{u} \right)^{\mathrm{T}} \right] \\ & + \boldsymbol{\nabla} (\lambda \boldsymbol{\nabla} \bullet \mathbf{u}) + \rho \mathbf{g} + \mathcal{Q}_{\mathbf{u}}. \end{aligned} \tag{2.21}$$

The momentum equation for viscous fluids is also called Navier-Stokes equation, of which there are many forms depending on the type of flow and the formulation. Eq. 2.21 is the conservative form of a momentum equation for a viscous Newtonian fluid.

2.2.1.4 The Energy Equation

In the sections above, derivations of the transport equations for mass, species and momentum were demonstrated starting from fundamental laws of physics. They fully describe the evolution of an isothermal system involving a single-phase that comprises multiple species. Many systems of technical relevance are non-isothermal, e.g. sprays, where droplet evaporation and subsequent mixture formation are considerably affected by temperature inhomogeneities. For such systems, an energy equation is needed for a complete description of the flow physics.

The energy equation can take many different forms such as the transport of total energy, internal energy, enthalpy or temperature. Here, the equation for sensible enthalpy is used,

of which a derivation following the same pattern as in the previous sections is tedious and beyond the scope of this thesis. For this reason, only some basic principles and the final form of the equation for sensible enthalpy are presented here. Rigorous derivations and comprehensive overviews of common forms of the energy equation can be found elsewhere [5, 8, 56, 65].

The basis of energy transport equations is the first law of thermodynamics, which states that the rate of change of the total energy E in a system is equal to the rate of which heat is added to the system $\dot{Q}$ and the rate of work done on the system $\dot{W}$, i.e.

$$\left(\frac{\mathrm{d}E}{\mathrm{d}t}\right)_{sys} = \dot{Q} + \dot{W}. \tag{2.22}$$

The rate of transferred heat can be divided into a heat flux across the boundaries $\dot{Q}_S$ and a source term $\mathcal{Q}_q$. Analogously, the rate of work is composed of the work done due to body forces $\dot{W}_b$ and the work due to surface forces $\dot{W}_s$. Moreover, the rate of work can be expressed in terms of force and velocity. Additional application of Reynolds' theorem 2.4 yields the final transport equation for the specific total energy

$$\frac{DE}{Dt} = \left[\boldsymbol{\nabla} \bullet (p\mathbf{u}) + \boldsymbol{\nabla} \bullet \boldsymbol{\tau} \bullet \mathbf{u}\right] + \mathbf{f_b} \bullet \mathbf{u} - \boldsymbol{\nabla} \bullet \dot{\mathbf{q}}_s + \mathcal{Q}_q, \tag{2.23}$$

where $\mathbf{f_b}$ and $\dot{\boldsymbol{q}}_s$ are the body force and heat flux vectors, respectively. In Eq. 2.23 the first term on the RHS (grouped by using square brackets) accounts for work by surface forces, the remaining terms on the RHS, from the left to the right, for work by body forces, heat flux and a heat source in the control volume, which corresponds to a coupling term to the dispersed phase in the context of multiphase systems.

The specific total enthalpy is defined as $h = e + p/\rho$, the sensible enthalpy as $h_s = h - \Delta h_f^o$, where Δh_f^o is the standard enthalpy of formation. Using these definitions as well as Eq. 2.23, Eq. 2.11, Eq. 2.19 yields (after numerous manipulations that can be found in the above-mentioned references)

$$\frac{\partial}{\partial t}(\rho h_s) + \boldsymbol{\nabla} \bullet (\rho \mathbf{u} h_s) = \frac{Dp}{Dt} + \boldsymbol{\nabla} \bullet (\alpha \boldsymbol{\nabla} \mathbf{u}) + \boldsymbol{\tau} : \boldsymbol{\nabla} \mathbf{u} + \mathcal{Q}_{h_s}, \tag{2.24}$$

where α is the thermal diffusivity and $\mathcal{Q}_{h_s}$ is a source term per unit volume that accounts for heat exchange between the continuous phase and the dispersed phase. It is important to note that the work due to gravitational forces has been omitted, assuming that the effect on enthalpy and temperature is negligible compared to other contributing terms in Eq. 2.24.

2.3 The Dispersed Phase

2.3.1 Number Density Functions

As mentioned previously, the focus of the present work in terms of modeling dispersed multiphase systems is placed on the representation of the particulate phase as a population of discrete elements. Let

$$\boldsymbol{\xi} = \begin{bmatrix} \xi_1, & \xi_2, & \ldots, & \xi_{N_d} \end{bmatrix}^{\mathrm{T}} \tag{2.25}$$

be a vector of internal coordinates, where each component ξ_i is a quantity characterizing an individual of the population. The first internal coordinate is typically the particle size. Other relevant properties, in particular with respect to sprays, are possibly the velocity components and temperature. If $\boldsymbol{\xi}$ contains all relevant physical properties, a complete description of a particulate system at every point in time, physical space and phase space (internal coordinate space) is given by a number density function (NDF) $n(\xi, \boldsymbol{x}, t)$, which is a non-negative function that maps N_d particle properties in the internal coordinate vector onto a particle number concentration. In other words, a NDF gives the concentration of particles with internal coordinate values lying in the interval $[\boldsymbol{\xi}, \boldsymbol{\xi} + \mathrm{d}\boldsymbol{\xi}]$. For the sake of convenience and readability, the NDF will henceforth be denoted simply by $n(\boldsymbol{\xi})$, $n_{\boldsymbol{\xi}}$ or n_{ξ} (depending on the actual or presumed dimensionality), omitting temporal and spatial dependencies.

2.3.2 The Population Balance Equation

As mentioned in the previous section, a NDF of a vector of relevant particle properties is sufficient to fully characterize a particulate system. Thus, in order to model the dispersed phase in a multiphase system, a mathematical description of the temporal and spatial evolution of the NDF is needed. Such a description is given in the form of a population balance equation (PBE), which is essentially a transport equation for the NDF in physical space and phase space. A well-known example of a PBE for spray applications is the Williams spray equation [95], which governs the evolution of reacting sprays. The equations and essential statements in this section are based on the excellent books of Marchisio and Fox [24, 52] and Ramkrishna [68]. The reader is referred to the original references for a comprehensive description and discussion of numerous aspects of population balances.

First, a slight change of notation from the previous sections is necessary: As the PBE is higher-dimensional compared to the previously presented transport equations and also relates to different spaces and control volumes, we introduce the notation $\Omega_{\mathbf{x}}$ and $\partial\Omega_{\mathbf{x}}$ for a finite control volume and its boundary in physical space, replacing V and S, respectively. Accordingly, a control volume in phase space is $\Omega_{\boldsymbol{\xi}}$ with the boundary $\partial\Omega_{\boldsymbol{\xi}}$. Moreover, the vector differential operator is subscripted with the vector/space that it operates on, i.e. $\boldsymbol{\nabla}_{\boldsymbol{\theta}} = \begin{bmatrix} \partial/\partial\theta_1, & \partial/\partial\theta_2, & \ldots, & \partial/\partial\theta_N \end{bmatrix}^{\mathrm{T}}$ for some vector $\boldsymbol{\theta}$ of arbitrary dimensionality N.

For the finite control volumes in physical space $\mathbf{x}$ and phase space $\boldsymbol{\xi}$, the PBE reads

$$\frac{\partial}{\partial t}\left(\int_{\Omega_{\boldsymbol{\xi}}}\int_{\Omega_{\mathbf{x}}} n_{\boldsymbol{\xi}}\,\mathrm{d}\mathbf{x}\,\mathrm{d}\boldsymbol{\xi}\right)+\int_{\Omega_{\boldsymbol{\xi}}}\oint_{\partial\Omega_{\mathbf{x}}}\left(n_{\boldsymbol{\xi}}\mathbf{u}\right)\mathrm{d}\mathbf{A}_{\mathbf{x}}\,\mathrm{d}\boldsymbol{\xi} + \int_{\Omega_{\mathbf{x}}}\oint_{\partial\Omega_{\boldsymbol{\xi}}}\left(n_{\boldsymbol{\xi}}\dot{\boldsymbol{\xi}}\right)\mathrm{d}\mathbf{A}_{\boldsymbol{\xi}}\,\mathrm{d}\mathbf{x}=\int_{\Omega_{\mathbf{x}}}\int_{\Omega_{\boldsymbol{\xi}}}\mathcal{Q}_{\boldsymbol{\xi}}\,\mathrm{d}\boldsymbol{\xi}\,\mathrm{d}\mathbf{x}, \tag{2.26}$$

where $\dot{\boldsymbol{\xi}}$ is the advection velocity in phase space, or in other words, a continous rate of change in the internal coordinates. The source term $\mathcal{Q}_{\boldsymbol{\xi}}$ accounts for discontinuous events such as aggregation and breakage. It shall remain an abstract term in this section but will be detailed in the context of drop breakup in Section 4.4.3.

It should be noted that there is no diffusion term in Eq. 2.26 although in general, diffusion can appear in the PBE. However, it is only relevant for very small particles (Marchisio and Fox [52] estimate sizes of less than one micron) or very low inertia. Hence, the effect of diffusive processes is assumed to be negligible for the applications of interest, namely sprays. In order to keep the complexity as low as possible, it is therefore omitted from the beginning. The surface integrals - as known from previous sections - can be transformed to volume integrals by means of Gauss' divergence theorem, which yields

$$\frac{\partial}{\partial t}\left(\int_{\Omega_{\boldsymbol{\xi}}}\int_{\Omega_{\mathbf{x}}} n_{\boldsymbol{\xi}}\,\mathrm{d}\mathbf{x}\,\mathrm{d}\boldsymbol{\xi}\right)+\int_{\Omega_{\boldsymbol{\xi}}}\int_{\Omega_{\mathbf{x}}}\boldsymbol{\nabla}_{\mathbf{x}}\bullet\left(\mathbf{u}n_{\boldsymbol{\xi}}\right)\mathrm{d}\mathbf{x}\,\mathrm{d}\boldsymbol{\xi} + \int_{\Omega_{\mathbf{x}}}\int_{\Omega_{\boldsymbol{\xi}}}\boldsymbol{\nabla}_{\boldsymbol{\xi}}\bullet\left(\dot{\boldsymbol{\xi}}n_{\boldsymbol{\xi}}\right)\mathrm{d}\boldsymbol{\xi}\,\mathrm{d}\mathbf{x}=\int_{\Omega_{\mathbf{x}}}\int_{\Omega_{\boldsymbol{\xi}}}\mathcal{Q}_{\boldsymbol{\xi}}\,\mathrm{d}\boldsymbol{\xi}\,\mathrm{d}\mathbf{x}, \tag{2.27}$$

Eq. 2.27 is satisfied for arbitrary control volumes $\Omega_{\mathbf{x}}$ and $\Omega_{\boldsymbol{\xi}}$ if

$$\frac{\partial n_{\boldsymbol{\xi}}}{\partial t}+\boldsymbol{\nabla}_{\mathbf{x}}\bullet\left(\mathbf{u}n_{\boldsymbol{\xi}}\right)+\boldsymbol{\nabla}_{\boldsymbol{\xi}}\bullet\left(\dot{\boldsymbol{\xi}}n_{\boldsymbol{\xi}}\right)=\mathcal{Q}_{\boldsymbol{\xi}}, \tag{2.28}$$

which is the differential form of a PBE. It is similar to the transport equations presented previously but contains an additional advection term in phase space.

The velocity vector $\mathbf{u}$ appears in the advection term in Eq. 2.26 - 2.28, i.e. the advection velocity in physical space is assumed to be known and equals the velocity of the continuous phase. However, in many applications of technical importance, e.g. sprays, that assumption is not justified. In those cases, the components of the advection velocity, henceforth denoted by $\mathbf{u_d}$, become internal coordinates, $\mathbf{u_d}\subset\boldsymbol{\xi}$, and the PBE reads

$$\frac{\partial n_{\boldsymbol{\xi}}}{\partial t}+\boldsymbol{\nabla}_{\mathbf{x}}\bullet\left(\mathbf{u}n_{\boldsymbol{\xi}}\right)+\boldsymbol{\nabla}_{\mathbf{u_d}}\bullet\left(\mathbf{a_d}n_{\boldsymbol{\xi}}\right)+\boldsymbol{\nabla}_{\boldsymbol{\xi}}\bullet\left(\dot{\boldsymbol{\xi}}n_{\boldsymbol{\xi}}\right)=\mathcal{Q}_{\boldsymbol{\xi}}, \tag{2.29}$$

where $\mathbf{a_d}$ is the particle acceleration. Eq. 2.29 is also referred to as generalized PBE [52].

A numerical solution of the PBE is possible with standard techniques such as finite volume, finite difference or finite element methods. However, the large number of dimensions involved in complex problems and the associated computational costs make such an approach prohibitive for most relevant applications. Thus, methods to approximate solutions to PBEs are required, which will be the main focus of Chapter 3.

2.4 Dimensionless Numbers

A system in fluid mechanics can often be characterized in terms of dimensionless numbers that relate the effects of different phenomena to one another. Table 2.1 contains the definitions of relevant dimensionless quatities as a basis for later considerations. The definitions often involve characteristic lengths, that are chosen differently depending on the type of flow. Here, we consistently use the particle diameter d as the characteristic length.

The Lewis number will be assumed to be unity in later sections, which is a common assumption for non-reactive systems. This also implies $Sc = Pr$. Moreover, as shown in Table 2.1, the Nusselt number and the Sherwood number can be expressed as functions of other dimensionless numbers. Here, both numbers are determined based on the widely used correlation given by Ranz and Marshall [69]:

$$Nu = 2 + 0.6Re^{1/2}Pr^{1/3}, \tag{2.30}$$

$$Sh = 2 + 0.6Re^{1/2}Sc^{1/3}. \tag{2.31}$$

The unity Lewis assumption yields $Nu = Sh$.

Table 2.1: Characteristic dimensionless quantities in dispersed multiphase flows. The thermal conductivity is denoted as κ, the convective heat transfer coefficient as h_c.

Dimensionless quantity	Definition	Physical interpretation
Reynolds number	$Re = \frac{d\rho u}{\mu}$	Relates inertial (destabilizing) to viscous (stabilizing) forces; indicator for the degree of turbulence.
Weber number	$We = \frac{d\rho u^2}{\sigma}$	Relates destabilizing inertial forces to stabilizing surface tension.
Ohnesorge number	$Oh = \frac{\mu_d}{\sqrt{\rho_d d\sigma}}$	Relates viscous forces to surface tension and inertial forces.
Prandtl number	$Pr = \frac{c_p\mu}{\kappa}$	Relates momentum diffusivity to thermal diffusivity.
Schmidt number	$Sc = \frac{\mu}{\rho\mathcal{D}}$	Relates momentum diffusivity to mass diffusivity.
Lewis number	$Le = \frac{\kappa}{\rho c_p \mathcal{D}} = \frac{Sc}{Pr}$	Relates thermal diffusivity to mass diffusivity.
Nusselt number	$Nu = \frac{h_c d}{\kappa} = f(Re, Pr)$	Relates convective to conductive heat transfer.
Sherwood number	$Sh = \frac{h_c d}{\mathcal{D}} = f(Re, Sc)$	Relates convective heat transfer to mass transport by diffusion.

3 Solution Approaches for Spray Systems

The equations presented in the previous chapter are generally valid for a dispersed multiphase system, where the particulate system can be described in terms of a PBE. While the basic approaches to approximate solutions to the PBE can be applied to systems with particles of an arbitrary state of matter, the physical relationships presented in this chapter are applicable specifically to sprays. Here, the term "spray" is used for a population of liquid droplets dispersed in a continuous gas phase.

First, a modified set of equations governing the evolution of the gas phase will be given in Section 3.1, since the general transport equations presented in the previous chapter are not suitable for the turbulent flows of interest. Following this, the relationships for the interaction of gas and single liquid drops are discussed in Section 3.2 before shifting the focus to the population scale.

A particular focus of this chapter are methods to approximate solutions to PBEs. Numerous methods exist to approach that problem, e.g. Monte Carlo methods, methods of moments, sectional methods. This thesis though, is primarily concerned with Lagrangian particle tracking (LPT) and quadrature-based moment methods (QBMM), which will be the subjects of Section 3.3 and Section 3.4, respectively. The references [52, 68] provide broad overviews of other methods such as the previously mentioned.

3.1 Gas Phase Equations

The transport equations presented in Chapter 2 fully describe the evolution of the continuous phase. However, analytical solutions exist only for very simple flow configurations, where the non-linear terms vanish. As such simplifications are not justified for typical problems occuring in nature and technology, the governing equations need to be solved numerically. In order to obtain reasonably accurate numerical solutions, the resolution in time and space must be sufficiently high to capture the phenomena on all relevant time and length scales.

An essential phenomenon in sprays as well as most technically important flows is turbulence. It occurs when inertial rather than viscous forces dominate the flow dynamics and is characterized by chaotic changes in the flow field due to irregular turbulent structures/eddies. Although the Navier-Stokes equations govern turbulent flows, the practical ability to solve them is limited by the degree of turbulence, namely the Reynolds number. This is due to the turbulent energy cascade that describes the transfer of energy from the large scales to the smallest scales where dissipation occurs (Kolmogorov scale). For a physically valid solution, the temporal and spatial resolution must be sufficient to capture

the entire range of scales, which increases with the Reynolds number [67], in the case of homogeneous isotropic turbulence according to the relation

$$\frac{l_0}{\eta} \sim Re^{-3/4}. \tag{3.1}$$

Here, l_0 and η denote the integral length scale and the Kolmogorov length scale, respectively. Considering three physical dimensions, Eq. 3.1 implies that the number of required discrete points for a numerical solution scales with $Re^{9/4}$.

Three main approaches exist for the numerical simulation of turbulent flows: (1) Direct numerical simulation (DNS), (2) Large-Eddy Simulation (LES) and (3) Reynolds-averaging. DNS is the most straightforward approach in the sense that is requires no turbulence modeling at all. However, it is limited to relatively low Reynolds numbers due to the above-described scaling problem. In LES, the large eddies, which contain the most energy, are resolved on the computational grid whereas the effect of small-scale turbulence is taken into account using subgrid-scale models (see Ref. [77] for a comprehensive description and discussion of LES).

Reynolds-averaging is the most advantageous method with respect to computational costs. It is suitable when numerical simulations aim at mean properties instead of turbulent fluctuations. Exhaustive descriptions and derivations of the Reynolds-averaged Navier-Stokes (RANS) equations[1] and related turbulence models can be found in the literature, e.g. [67, 93]. Summarized briefly, the RANS equations are based on the decomposition of a field variable ϕ into a mean component $\langle\phi\rangle$ and a fluctuating component ϕ'. That is, the velocity in ith direction can be expressed as

$$u_i = \langle u_i \rangle + u_i'. \tag{3.2}$$

This approach results in a closure problem when Eq. 3.2 is substituted into the momentum equation. More precisely, the term

$$\tau_{ij}' = -\overline{u_i' u_j'} \tag{3.3}$$

appears in the averaged momentum equation. It is referred to as the Reynolds stress tensor and needs to be closed by a suitable turbulence model. A variety of turbulence models exist to close the RANS equations. One of the most common models is the $k-\epsilon$ turbulence model, which is also used here. Like numerous other turbulence models, the underlying assumption of the model is that momentum transfer by turbulent structures can be modeled with a turbulent viscosity (also referred to as eddy viscosity), here denoted as μ_t, which is also known as the Boussinesq assumption. The $k-\epsilon$ model specifically uses the correlation

$$\mu_t = C_\mu \rho \frac{k^2}{\epsilon}, \tag{3.4}$$

[1]The term "Navier-Stokes equations" originally refers to the momentum equation. However, in the broader sense it is used for the governing equations in CFD in general, especially in the context of RANS.

where k and ϵ are the turbulent kinetic energy and dissipation rate, respectively. C_μ is a constant that is usually set equal to 0.09. In order to obtain closure, two additional transport equations for k and ϵ are introduced, that contain several new terms that have to be modeled. For this reason the additional transport equations are omitted here. A thorough description can be found in [67, 89].

Since the density in variable-density flows would introduce additional unclosed terms in the RANS equations, Favre-averaging (density-weighted averaging), denoted by a tilde, is used instead of Reynolds-averaging. This kind of averaging is described in detail in Ref. [93].

Using a Reynolds-averaged density $\overline{\rho}$, Favre-averaging for the remaining field variables and the definition of turbulent viscosity in Eq. 3.4, we can finally write the governing equations of the problems investigated in this thesis:

1. Continuity equation

$$\frac{\partial \overline{\rho}}{\partial t} + \boldsymbol{\nabla} \bullet (\overline{\rho}\widetilde{\mathbf{u}}) = \mathcal{Q}_\rho \tag{3.5}$$

2. Species equation

$$\frac{\partial}{\partial t}\left(\overline{\rho}\widetilde{Y}_i\right) + \boldsymbol{\nabla} \bullet \left(\overline{\rho}\widetilde{Y}_i\right) = \boldsymbol{\nabla} \bullet \left[(\mu + \mu_t)\,\boldsymbol{\nabla} Y_i\right] + \mathcal{Q}_{Y_i} \tag{3.6}$$

3. Momentum equation

$$\begin{aligned}\frac{\partial}{\partial t}(\overline{\rho}\widetilde{\mathbf{u}}) + \boldsymbol{\nabla} \bullet (\overline{\rho}\widetilde{\mathbf{u}}\widetilde{\mathbf{u}}) = &- \boldsymbol{\nabla}\overline{p} + \boldsymbol{\nabla} \bullet \left[(\mu + \mu_t)\boldsymbol{\nabla}\widetilde{\mathbf{u}}\right] \\ &+ \boldsymbol{\nabla} \bullet \left[(\mu + \mu_t)\left(\boldsymbol{\nabla}\widetilde{\mathbf{u}}\right)^{\mathrm{T}}\right] - \boldsymbol{\nabla}\left[\tfrac{2}{3}(\mu + \mu_t)\boldsymbol{\nabla} \bullet \widetilde{\mathbf{u}}\right] \\ &+ \overline{\rho}\mathbf{g} + \mathcal{Q}_{\mathbf{u}}.\end{aligned} \tag{3.7}$$

4. Sensible enthalpy equation

$$\frac{\partial}{\partial t}\left(\overline{\rho}\widetilde{h}_s\right) + \boldsymbol{\nabla}\left(\overline{\rho}\widetilde{\mathbf{u}}\widetilde{h}_s\right) = \frac{\mathrm{D}\overline{p}}{\mathrm{D}t} + \boldsymbol{\nabla} \bullet \left[(\alpha + \alpha_t)\boldsymbol{\nabla}\widetilde{h}_s\right] + \mathcal{Q}_{h_s} \tag{3.8}$$

It should be noted that the species diffusivity in Eq. 3.6 is assumed equal to the kinematic viscosity, i.e. $\mathcal{D} = \mu/\rho$. As for the turbulent thermal diffusivity α_t, a simple linear dependence on μ_t is assumed.

The Eqs. 3.5-3.8 are solved in a discretized form with the finite volume method (FVM), using the open source CFD code FOAM-extend, an edition of OpenFOAM®. For detailed information on discretization schemes and the FVM, the reader is referred to [56, 89].

3.2 Droplet-Gas Interaction

Before dealing with methods to approximate solutions to PBEs, the correlations for droplet-gas interactions shall be described briefly. The following three main assumptions/limitations underlie the considerations in Section 3.2.1 - 3.2.3:

1. The conditions are typical for sprays, defined as liquid injected into gas of the same or a higher temperature, i.e. $T_d \leq T_c$, $u_d \leq u_c$. It is particularly important to note that mass exchange can take place only from the droplets to the gas. While the models for momentum and heat exchange are theoretically valid in both directions, the mass exchange is modeled specifically for the case of evaporating droplets and does not include condensation.
2. Each entity of the population can be treated as an isolated particle. Droplet-droplet interaction occurs only via coupling with the continuous phase.[2] This is a common, albeit strong assumption that mainly originates from the fact that experimental and theoretical investigations are usually conducted on single droplets.
3. Droplets are considered homogeneous. The internal drop velocity is equal to the surface velocity and heat conduction within the drop is infinitely fast.

Based on these statements, the correlations for mass, heat and momentum exchange between entities of the dispersed system and surrounding gas are described below. Properties of the dispersed phase and the continuous phase are henceforth denoted by the subscripts d and c, respectively.

3.2.1 Mass Exchange

The mass flow across the droplet-gas interface due to evaporation is described by

$$\frac{\mathrm{d}m_d}{\mathrm{d}t} = -Sh\pi r_d \mathcal{D}\rho_c \ln(1 + B_m), \tag{3.9}$$

where r_d is the droplet radius, $\mathcal{D}$ the mass diffusivity and B_m the Spalding mass transfer number defined as

$$B_m = \frac{Y_{vs} - Y_{v\infty}}{1 - Y_{vs}}, \tag{3.10}$$

where Y_{vs} and $Y_{v\infty}$ are the vapor mass fraction at the droplet surface and far from the droplet surface, respectively. A common method to determine the mass fractions is the calculation from partial pressures based on a vapor-liquid-equilibrium. Eq. 3.9

[2] The only direct droplet-droplet interaction in sprays that is sometimes considered, typically with a stochastic approach, is coalescence as a consequence of collisions. However, collisions are not subject of this thesis and will therefore not be addressed any further.

is well-established and commonly applied to model liquid droplet evaporation. Verbose derivations can be found elsewhere, e.g. [80, 82].

With a unity Lewis number assumption, we can write

$$\frac{\kappa_c}{c_p} = \rho_c \mathcal{D}, \tag{3.11}$$

where κ_c is the gas thermal conductivity and c_p is the gas heat capacity at constant pressure. Substituting Eq. 3.11 into Eq. 3.9 and expressing the droplet size in terms of the droplet diameter $d_d = r_d$ yields

$$\frac{\mathrm{d}m_d}{\mathrm{d}t} = -Sh\pi d_d \frac{\kappa_c}{c_p} \ln(1 + B_m). \tag{3.12}$$

Furthermore, we assume that the shape of droplets is spherical:

$$\frac{\mathrm{d}m_d}{\mathrm{d}t} = \frac{\pi}{6} \frac{\mathrm{d}(\rho_l d_d^3)}{\mathrm{d}t}\,. \tag{3.13}$$

Collecting altogether, we obtain the expression for the rate of change in droplet diameter

$$\frac{\mathrm{d}d_d}{\mathrm{d}t} = -2Sh \frac{1}{d_d} \frac{\kappa_c}{c_p \rho_c} \ln(1 + B_m) - \frac{1}{3} \frac{d_d}{\rho_d} \frac{\mathrm{d}\rho_d}{\mathrm{d}t}\,. \tag{3.14}$$

The first term on the RHS represents the shrinking of the droplet by evaporation at a constant temperature and tends to infinity for small droplets. The second term on the RHS accounts for thermal expansion due to temperature changes.

The properties κ_c, c_p and ρ_c are the thermophysical properties of the continuous phase in the vicinity of the evaporating droplet. They depend on composition Y_i and temperature T, properties that are unknown in the critical film region. A common modeling approach is to assume spatially constant reference properties of the gas-vapor mixture. Several empirical rules exist for that purpose. In the present study, the 1/3 rule is employed for both the reference temperature and reference species mass fractions as suggested by Hubbard et al. [37]:

$$\begin{aligned} T_{ref} &= T_s + \frac{1}{3}\left(T_s - T_\infty\right), \\ Y_{i,ref} &= Y_s + \frac{1}{3}\left(Y_{i,s} - Y_{i,\infty}\right), \end{aligned} \tag{3.15}$$

where the subscript ∞ indicates a property far from the drop surface.

3.2.2 Heat Exchange

The heat exchange between droplets and gas results from the energy conservation equation

$$m_d \frac{\mathrm{d}}{\mathrm{d}t}\left[c_l\left(T_d - T_{ref}\right)\right] = \dot{Q}_d + \frac{\mathrm{d}m_d}{\mathrm{d}t} h_v(T_d), \tag{3.16}$$

where c_l denotes the specific heat capacity of the liquid drop, T_d the droplet temperature, T_{ref} the reference temperature as defined in Eq. 3.15, $\dot{Q}_d$ the heat flux across the surface and h_v the latent heat of vaporization. Evidently, both the gas-to-droplet heat transfer and the mass transfer contribute to the change of drop temperature. Hence, heat transfer is coupled to mass transfer (Eq. 3.12), which is a problem that is commonly approached by introducing a correction factor f into the heat flux eqauation

$$\dot{Q}_d = \pi d_d \kappa_c Nu f (T_c - T_d). \tag{3.17}$$

With the definition

$$z = \frac{\mathrm{d}m_d}{\mathrm{d}t} \frac{c_p}{\pi d_d \kappa_c Nu} \tag{3.18}$$

the correction factor can be expressed as

$$f = \frac{z}{e^z - 1}. \tag{3.19}$$

This approach is based on the energy balance at the droplet surface. A thorough derivation is given in Ref. [79]. The rate of change in droplet temperature can finally be written simply as

$$\frac{\mathrm{d}T_d}{\mathrm{d}t} = \frac{\dot{Q}_d}{c_l m_d}. \tag{3.20}$$

3.2.3 Momentum Exchange

The rate of velocity change of a spherical droplet is governed by the momentum balance [82]

$$m_d \frac{\mathrm{d}\mathbf{u_d}}{\mathrm{d}t} = \frac{1}{2} \rho_c C_d r_d^2 \|\mathbf{u_c} - \mathbf{u_d}\| (\mathbf{u_c} - \mathbf{u_d}), \tag{3.21}$$

where C_d is the drag coefficient. Substituting Eq. 3.13 into Eq. 3.21 and rearranging yields the droplet acceleration

$$\frac{\mathrm{d}\mathbf{u_d}}{\mathrm{d}t} = \frac{1}{d_d} \frac{3}{4} \frac{\rho_c}{\rho_d} C_d \|\mathbf{u_c} - \mathbf{u_d}\| (\mathbf{u_c} - \mathbf{u_d}). \tag{3.22}$$

The drag force is linearly dependent on the drag coefficient C_d and various correlations exist for the choice of it. A widely used correlation is

$$C_d = \begin{cases} \frac{24}{Re} \left(1 + \frac{1}{6} Re^{2/3}\right) & \text{if} \quad Re \leq 1000 \\ 0.44 & \text{otherwise.} \end{cases} \tag{3.23}$$

The Reynolds number to determine the drag coefficient is calculated using the reference properties of the mixture (Eq. 3.15) to account for the effects of evaporation. Additionally, if evaporation is present, it is possible to model the effect of Stefan convection[3], e.g. by correcting the drag coefficient with a factor $1/(1 + B_m)$ [82].

[3] Stefan convection is a term describing phase-change induced convection.

3.3 Lagrangian Particle Tracking

One of the most common techniques to approximate solutions to PBEs, especially for sprays, is the representation of a population by a large number of randomly seeded discrete particles interacting with the continuous gas phase that is described by Eulerian field equations. This Monte-Carlo approach is commonly referred to as Eulerian-Lagrangian modeling or Lagrangian particle tracking (LPT). The representation of particles by discrete Lagrangian parcels is intuitive and enables a simple implementation. Despite its limitations, which will be addressed at the end of this section, it has remained one of the (if not the) most frequently applied method for spray simulations.

The solution technique is relatively straightforward. Droplets are modeled by discrete particles, so-called Lagrangian parcels, that are defined in terms of diameter, mass, temperature, velocity and other characteristic droplet properties. One parcel can represent an arbitrary number of droplets that directly results from mass and diameter. In other words, one parcel represents a random interval of a multivariate NDF. A particular benefit of this approach is that there is practically no limit to the dimensionality of the NDF, since a high number of internal coordinates can be assigned to the parcels. Examples of additional variables associated with a Lagrangian parcel are the drop deformation, characteristic time scales or liquid composition.

The parcels are tracked individually and consecutively by numerically solving the equations given in Section 3.2. The source terms in Eqs. 3.5 - 3.8 are then obtained on a per-cell basis from

$$\mathcal{Q}_{\rho}^{(j)} \approx \sum_{k=1}^{N_j} \frac{1}{\Delta V_j} \frac{\mathrm{d}m_{d,k}}{\mathrm{d}t} \Delta t, \tag{3.24}$$

$$\mathcal{Q}_{Y_i}^{(j)} \approx \sum_{k=1}^{N_j} \frac{1}{\Delta V_j} \frac{\mathrm{d}(m_{d,k} Y_{i,k})}{\mathrm{d}t} \Delta t, \tag{3.25}$$

$$\mathcal{Q}_{\mathbf{u}}^{(j)} \approx \sum_{k=1}^{N_j} \frac{1}{\Delta V_j} \left(m_{d,k} \frac{\mathrm{d}\mathbf{u_{d,k}}}{\mathrm{d}t} + \mathbf{u_{d,k}} \frac{\mathrm{d}m_{d,k}}{\mathrm{d}t} \right) \Delta t, \tag{3.26}$$

$$\mathcal{Q}_{h_s}^{(j)} \approx \sum_{k=1}^{N_j} \frac{1}{\Delta V_j} c_l \left(m_{d,k} \frac{\mathrm{d}T_{d,k}}{\mathrm{d}t} + T_{d,k} \frac{\mathrm{d}m_{d,k}}{\mathrm{d}t} \right) \Delta t, \tag{3.27}$$

where j denotes the index of the numerical grid cell (Eulerian frame of reference) and k the index of one of N_j Lagrangian parcels in the jth cell. In Eq. 3.27, the specific heat capacity of the liquid c_l is assumed constant. The basic LPT procedure including the transfer of heat, mass and momentum to a computational cell of the Eulerian grid is illustrated in Figure 3.1. In addition to the transfer of mass, momentum and heat, other models can be applied to each individual parcel. Examples are collision models, wall models, turbulent dispersion models and atomization models, some of which will be discussed in Section 4.4.2.

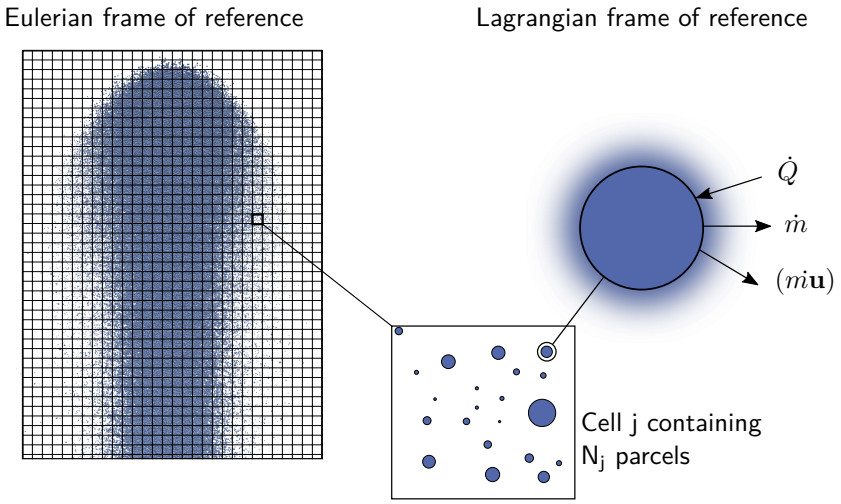

Figure 3.1: *Schematic illustration of Euler-Lagrange modeling*

The Lagrangian modeling approach is intuitive, straightforward and well-established. Another reason for the frequent application of LPT to sprays is the good compatibility with RANS turbulence modeling and the associated low numerical costs. However, it has several limitations and disadvantages: First, the applicability of LPT - while maintaining reasonable accuracy - is limited to relatively low volume fractions of the dispersed phase (a frequently stated limit is 10 %). This is a problem in spray applications, where the liquid volume fraction in close proximity of the nozzle is relatively high. This generally causes a strong grid dependence of Euler-Lagrange methods. Moreover, a sufficient resolution of the NDF/PBE usually requires a large number of parcels. Most spray applications exhibit high droplet concentrations only in small parts of the domain. This leads to a strong imbalance in large-scale simulations, where parallelization is usually achieved by domain decomposition. From this perspective, purely Eulerian methods are desirable, as they offer a much better scalability in parallel simulations.

3.4 Quadrature-Based Moment Methods

As stated in Section 2.3.2, the evolution of a particulate system is completely described by a PBE if the transported NDF is a function of all relevant particle properties. Solving a PBE with numerical methods is possible. However, most of the multiphase flows occurring in nature and technology are only adequately described by a multivariate NDF, where the high dimensionality entails computational costs that make a direct numerical solution of the PBE practically impossible.

A relatively new family of methods to approach that problem are the quadrature-based moment methods (QBMM). They are suitable if integral properties of the NDF suffice to capture the effect of the particulate phase on the continuous phase or the system, which is the case for many spray applications. A well-konwn example of such an application is the injection of liquid fuel in propulsion systems, where local mixture fractions and temperatures are affected by the integral spray source terms. The fundamental idea and few specific types of QBMM are described below. For simplicity, the considerations will be restricted to univariate NDFs (until Section 3.4.4) with the size as the only internal coordinate, i.e. $\boldsymbol{\xi} = \xi = d$.

3.4.1 The Moment Transport Equation

The kth moment of a continuous, univariate density function $n(\xi)$ is defined as

$$c_k = \int_{\Omega_\xi} \xi^k n(\xi)\,\mathrm{d}\xi. \tag{3.28}$$

An approximation to the PBE solution is obtained by numerically solving a transport equation not for the NDF but for a number of its moments. The derivation of the moment transport equations is straightforward. Multiplying Eq. 2.28 by ξ^k and integrating with respect to ξ yields

$$\int_{\Omega_\xi} \xi^k \frac{\partial n_\xi}{\partial t}\,\mathrm{d}\xi + \int_{\Omega_\xi} \xi^k \boldsymbol{\nabla}_\mathbf{x} \bullet \left(\mathbf{u} n_\xi\right)\mathrm{d}\xi + \int_{\Omega_\xi} \xi^k \frac{\partial}{\partial \xi}\left(\dot{\xi} n_\xi\right)\mathrm{d}\xi = \int_{\Omega_\xi} \xi^k \mathcal{Q}_\xi\,\mathrm{d}\xi. \tag{3.29}$$

As t, $\mathbf{x}$ and ξ are independent coordinate spaces, the partial derivatives in the first two terms on the LHS can be separated from the integrand. Additionally considering the moment definition in Eq. 3.28 and applying integration by parts to the third term on the LHS yields the transport equation for the kth moment

$$\frac{\partial c_k}{\partial t} + \boldsymbol{\nabla}_{\boldsymbol{x}}\left(\mathbf{u} c_k\right) = -\left.\dot{\xi} n_\xi \xi^k\right|_0^{\xi_{max}} + \int_0^{\xi_{max}} k\xi^{k-1}\dot{\xi} n_\xi\,\mathrm{d}\xi + \mathcal{Q}_{c,k}, \tag{3.30}$$

where the moment transform of the source term due to discontinuous events (RHS in Eq. 3.29) has been substituted with $\mathcal{Q}_{c,k}$. For now, we can assume the absence of such events, i.e. $\mathcal{Q}_{c,k} = 0$.

For the number of transported moments tending to infinity, the moment set is unique for an arbitrary NDF. However, it is assumed that a relatively small number of transported moments is sufficient to approximate the quantities of interest with adequate accuracy.

Eq. 3.30 is unclosed, as the source term $\dot{\xi}$ is usually a function of ξ and cannot be expressed in terms of the kth moment itself. In order to obtain closure, several QBMM were developed, of which two, namely the QMOM and the EQMOM, are described in the following sections.

3.4.2 The Quadrature Method of Moments (QMOM)

Presuming a known advection velocity in physical space, the closure problem in the moment transport equations reduces to the problem of finding a physically consistent set of moment source terms from the original moment set, which results from discontinuous processes and the advection in phase space. A suitable method to obtain closure for the moment transport equations is the quadrature method of moments (QMOM) [54], which makes use of the Gaussian quadrature to achieve a maximum degree of accuracy for a given number of transported moments.

The QMOM is based on the fundamental assumption that the NDF is a continous function on the support interval. Hence, it can be approximated by a polynomial function[4]. An integral of the form $\int n(\xi)g(\xi)$ can then be approximated by an N-point quadrature

$$\int_{\Omega_\xi} n(\xi)g(\xi)\,\mathrm{d}\xi \approx \sum_{\alpha=1}^{N} w_\alpha g(\xi_\alpha), \tag{3.31}$$

where w_α and ξ_α are the weights and nodes of the qudrature, respectively. The quadrature is said to be a Gaussian quadrature if it has an accuracy of $2N-1$, i.e. there exists at least one polynomial of order $2N$ that makes the quadrature inexact (assuming the integrand is a polynomial). Considering the definition of moments in Eq. 3.28, it is obvious that for the kth moment

$$g(\xi) = \xi^k. \tag{3.32}$$

The N quadrature weights and nodes can thus be determined from the first $2N$ moments by solving a system of nonlinear equations:

$$\begin{aligned} c_0 &= \sum_{\alpha=1}^{N} w_\alpha \\ c_1 &= \sum_{\alpha=1}^{N} w_\alpha \xi_\alpha \\ &\vdots \\ c_{2N-1} &= \sum_{\alpha=1}^{N} w_\alpha \xi_\alpha^{2N-1}. \end{aligned} \tag{3.33}$$

The integral approximation obtained by solving the equation system above is a Gaussian quadrature because it has an accuracy of $2N-1$ and only a Gaussian quadrature is able to capture moments up to the order of $2N-1$ [52]. Proof of Eq. 3.33 yielding a Gaussian quadrature can be found in Ref. [27].

[4]The Weierstrass theorem or Stone-Weierstrass theorem states that any continuous function on a real interval can be approximated by a polynomial as closely as desired.

Eq. 3.33 could be solved by any non-linear equation solver. However, convergence is not guaranteed without a good initial guess. Instead, another property of Gaussian quadratures, which involves orthogonal polynomials, is made use of. Per definition, the nodes of a Gaussian quadrature are the roots of an orthogonal set of polynomials with respect to $n(\xi)$. A set of polynomials $P_0(\xi), P_1(\xi) \dots P_\alpha(\xi)$ is orthogonal in the integration interval Ω_ξ with respect to $n(\xi)$ if

$$\int_{\Omega_\xi} n(\xi) P_\alpha(\xi) P_\beta(\xi) \, \mathrm{d}\xi = 0, \qquad \alpha \neq \beta, \tag{3.34}$$

where

$$P_\alpha(\xi) = k_{\alpha,0}\xi^\alpha + k_{\alpha,1}\xi^{\alpha-1} + \ldots + k_{\alpha,\alpha-1}\xi + k_{\alpha,\alpha}. \tag{3.35}$$

The most important property of orthogonal polynomials that is exploited to determine the weights and nodes of a Gaussian quadrature is a recursive relation. That is, a polynomial in a set of orthogonal polynomials can be determined from the two lower order polynomials by applying the recurrence formula

$$P_{\alpha+1}(\xi) = (\xi - a_\alpha) P_\alpha(\xi) - b_\alpha P_{\alpha-1}(\xi), \tag{3.36}$$

where

$$\begin{aligned}
&P_{-1}(\xi) = 0, \\
&P_0(\xi) = 1, \\
&a_\alpha = \frac{\int_{\Omega_\xi} n(\xi)\xi P_\alpha(\xi) P_\alpha(\xi) \, \mathrm{d}\xi}{\int_{\Omega_\xi} n(\xi) P_\alpha(\xi) P_\alpha(\xi) \, \mathrm{d}\xi}, \\
&b_\alpha = \frac{\int_{\Omega_\xi} n(\xi) P_\alpha(\xi) P_\alpha(\xi) \, \mathrm{d}\xi}{\int_{\Omega_\xi} n(\xi) P_{\alpha-1}(\xi) P_{\alpha-1}(\xi) \, \mathrm{d}\xi}.
\end{aligned}$$

The recursive relationship can be applied to compute the quadrature nodes [18]. Writing Eq. 3.36 in matrix form yields

$$\xi \begin{bmatrix} P_0(\xi) \\ P_1(\xi) \\ \vdots \\ P_{N-2}(\xi) \\ P_{N-1}(\xi) \end{bmatrix} = \begin{bmatrix} a_0 & 1 & & & \\ b_1 & a_1 & 1 & & \\ & \ddots & \ddots & \ddots & \\ & & \ddots & a_{N-2} & 1 \\ & & & b_{N-1} & a_{N-1} \end{bmatrix} \begin{bmatrix} P_0(\xi) \\ P_1(\xi) \\ \vdots \\ P_{N-2}(\xi) \\ P_{N-1}(\xi) \end{bmatrix} + \begin{bmatrix} 0 \\ 0 \\ \vdots \\ 0 \\ P_N(\xi) \end{bmatrix}. \tag{3.37}$$

As illustrated in Eq. 3.37, the quadrature nodes are the eigenvalues of the tridiagonal matrix. Moreover, Wilf [94] showed that the quadrature weights can be determined from elements of its eigenvectors. Transforming the tridiagonal matrix in Eq. 3.37 to a

symmetric matrix by a similarity transformation, the entire moment inversion problem reduces to finding the eigenvalues and eigenvectors of a symmetric tridiagonal matrix of the form

$$\begin{bmatrix} a_0 & \sqrt{b_1} & & \\ \sqrt{b_1} & \ddots & \ddots & \\ & \ddots & a_{N-2} & \sqrt{b_{N-1}} \\ & & \sqrt{b_{N-1}} & a_{N-1} \end{bmatrix}. \tag{3.38}$$

In practice, this matrix and consequently the recursion coefficients a_α and b_α to eventually obtain the quadrature, are computed by specialized algorithms such as the product-difference algorithm [28] or the Wheeler algorithm [76].

3.4.3 The Extended Quadrature Method of Moments (EQMOM)

For the standard QMOM to give the desired high accuracy, a large number of transported moments may be required. This does not only result in many additionional transport equations but can also lead to an ill-conditioned moment-inversion problem. Moreover, the modeling of some physical processes requires pointwise values of the NDF, which are unavailable in standard QMOM, where the discrete quadrature nodes essentially correspond to Dirac Delta functions. In cases where the PBE contains a negative growth term, i.e. evaporating droplets, the NDF is shifted along the negative internal-coordinate-axis and $n(\xi = 0)$ must be known for a physically correct closure of the moment transport equations. For such cases, Yuan et al. [100] extended the QMOM to allow a reconstruction of the NDF by the implementation of so-called kernel density functions (KDF) with a presumed shape instead of Dirac Delta functions. The NDF is then approximated by

$$n(\xi) = \sum_{\alpha=1}^{N} w_\alpha \delta_\sigma(\xi; \xi_\alpha), \tag{3.39}$$

where α denotes the quadrature node index and δ_σ a presumed KDF with the shape parameter σ, which raises the number of unknown variables in the moment-inversion problem to $2N + 1$. Hence, one additional moment is required for the EQMOM.

The choice of KDFs depends primarily on the support. If the internal coordinate is bounded, a beta distribution is an appropriate choice for δ_σ, as it is defined on the interval $\xi = [0, 1]$. The transformation between KDF space and physical space is straightforward.

For the following considerations, a beta distribution is chosen as the KDF. The procedure is analogous for other distributions that can be transformed to a weight function of a known set of orthogonal polynomials. Previously applied kernels are beta and gamma kernels [100], lognormal kernels [50] and more recently Laplace and Weibull kernels [62].

Presuming a beta distribution to be the KDF, the approximation of the NDF is

$$n(\xi) = \sum_{\alpha=1}^{N} w_\alpha \frac{\xi^{\lambda_\alpha - 1}(1-\xi)^{\mu_\alpha - 1}}{B(\lambda_\alpha, \mu_\alpha)}, \tag{3.40}$$

where

$$\lambda_\alpha = \frac{\xi_\alpha}{\sigma}, \qquad \mu_\alpha = \frac{1-\xi_\alpha}{\sigma}$$

and $B(\lambda_\alpha, \mu_\alpha)$ is the beta function.

For a beta KDF, the moments can be determined by application of a recursion formula $c_k(\xi_\alpha, \sigma, c_{k-1})$, and the NDF moments are found from a weighted sum of the KDF moments. Combining altogether yields

$$c_k = \begin{cases} 1, & k = 0 \\ \displaystyle\sum_{\alpha=1}^{N} w_\alpha \prod_{i=0}^{k-1} \left(\frac{\xi_\alpha + i\sigma}{1 + i\sigma} \right), & k > 0. \end{cases} \tag{3.41}$$

Introducing the definition of c_k^* as the kth moment determined with a standard QMOM approximation ($\sigma = 0$)

$$c_k^* = \sum_{\alpha=1}^{N} w_\alpha \xi_\alpha^k, \tag{3.42}$$

c_k can be transformed to c_k^* and vice versa by solving a system of linear equations

$$\begin{aligned} \mathbf{c} &= \mathbf{A}(\sigma)\mathbf{c}^*, \\ \mathbf{c}^* &= \mathbf{A}(\sigma)^{-1}\mathbf{c}. \end{aligned} \tag{3.43}$$

In practice, σ is found from an iterative procedure in such a way that c_{2N}^* computed from the EQMOM approximation based on the first $2N-1$ moments matches the last transported moment, i.e.

$$J_n(\sigma) = c_{2n} - \gamma_{2n} c_{2n}^* - \ldots - \gamma c_1^* \approx 0, \tag{3.44}$$

where γ_k ($k = 1 \ldots 2n$) are non-negative coefficients depending only on σ. Then σ is found as the smallest value for which Eq. 3.44 is satisfied. A more detailed description of the steps above can be found in Ref. [100, 101]. The iterative moment inversion procedure is illustrated in Fig. 3.2.

Closure of the moment equations, which is the general purpose of QBMM, can be achieved by the use of a so-called second quadrature $(\xi_{\alpha\beta}, w_{\alpha\beta})$, which is constructed based on the first quadrature, taking advantage of the properties of known orthogonal polynomials. In case of a presumed beta distribution, the suitable family of polynomials are the Jacobi

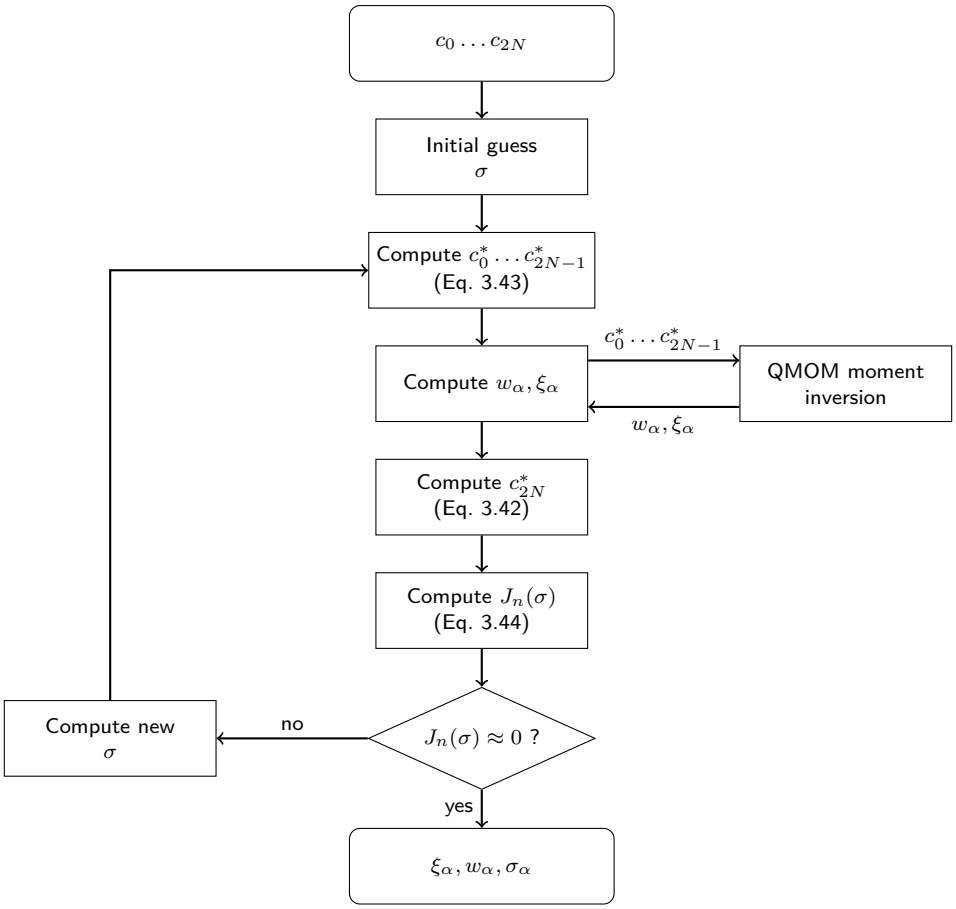

Figure 3.2: *The EQMOM moment inversion algorithm, cf. Ref. [100]*

polynomials, as they are orthogonal on the interval $(-1, 1)$ with respect to the weight function

$$w(t) = (1-t)^a(1+t)^b. \tag{3.45}$$

Using Eq. 3.40, the change of variable

$$\xi = \frac{t+1}{2} \tag{3.46}$$

and the parameters $a_\alpha = \mu_\alpha - 1$ and $b_\alpha = \lambda_\alpha - 1$ yield the integral expression

$$\int_0^1 g(\xi)\delta_\sigma(\xi;\xi_\alpha,\sigma) = \left(\frac{1}{2}\right)^{a_\alpha+b_\alpha+1} \frac{1}{B(\mu_\alpha,\lambda_\alpha)} \int_{-1}^1 g\left(\frac{t+1}{2}\right) w_\alpha(t)\,\mathrm{d}t, \tag{3.47}$$

where $g(\xi)$ is an arbitrary function corresponding to Eq. 3.31 and $w_\alpha(t)$ is the weight function with the parameters a_α and b_α.

The great advantage of the transformation into the weight function for Jacobi polynomials is that an arbitrary number of second quadrature nodes for each first quadrature node can be computed efficiently, as the recursion coefficients, i.e. the matrix in Eq. 3.38, are known beforehand. It is thus not required to invert a larger set of moments. With N_α known second quadratures for each KDF, the integral in Eq. 3.47 can be approximated by

$$\int_0^1 g(\xi)\delta_\sigma(\xi;\xi_\alpha,\sigma) \approx \sum_{\beta=1}^{N_\alpha} w_{\alpha\beta} g(\xi_{\alpha\beta}) = \sum_{\beta=1}^{N_\alpha} w_{\alpha\beta} g\left(\frac{t_{\alpha\beta}+1}{2}\right). \tag{3.48}$$

The integral with respect to the complete NDF on an interval $[\xi_0, \xi_1]$ can then be expressed as

$$\begin{aligned}\int_{\xi_0}^{\xi_1} g(\xi)n(\xi)\,\mathrm{d}\xi &= \int_{\xi_0}^{\xi_1} g(\xi) \sum_{\alpha=1}^{N} w_\alpha \delta_\sigma(\xi;\xi_\alpha)\,\mathrm{d}\xi \\ &= \sum_{\alpha=1}^{N}\sum_{\beta=1}^{N_\alpha} w_\alpha w_{\alpha\beta} g(\xi_{\alpha\beta}) I_{[\xi_0,\xi_1]}(\xi_{\alpha\beta}),\end{aligned} \tag{3.49}$$

where $I_{[\xi_0,\xi_1]}$ denotes the indicator function on the interval $[\xi_0, \xi_1]$, of which the form depends on the chosen KDF. In beta EQMOM, it corresponds to the incomplete beta function.

While the integral term in the moment equation (Eq. 3.30, second term on the RHS) is closed by Eq. 3.49, closure for the growth term is achieved using a pointwise representation of the NDF

$$n(\xi) = \sum_{\alpha=1}^{N}\sum_{\beta=1}^{N_\alpha} w_\alpha w_{\alpha\beta}\delta(\xi - \xi_{\alpha\beta}), \tag{3.50}$$

which corresponds to a standard QMOM representation with the second quadrature. With a known relationship for the physical source term (e.g. Eq. 3.14)

$$\frac{\mathrm{d}\xi_{\alpha\beta}}{\mathrm{d}t} = \dot{\xi}(\xi_{\alpha\beta}) = g(\xi_{\alpha\beta}), \tag{3.51}$$

Eq. 3.30 is fully closed. The use of the second quadrature clearly illustrates the advantages of the EQMOM. The method is applicable in cases where pointwise values of the NDF are required to close the moment equations. Additionally, EQMOM offers the possibility to arbitrarily increase the number of second quadrature nodes for cases with a strong non-linear dependence of $\dot{\xi}$ on ξ.

3.4.4 Multivariate QBMM

Up to this point, QBMM were presented for the case of a univariate NDF, i.e. size was considered as the only internal coordinate. However, detailed spray modeling requires

additional properties as elements of the internal coordinate vector, in other words, a multivariate NDF is needed. For such cases to be modeled with QBMM, moments of higher dimensions as well as mixed moments are needed. A mixed moment of order $k_1, k_2 \ldots, k_{N_d}$ of a continuous N_d-dimensional NDF is defined as

$$c_{k_1,k_2\ldots,k_{N_d}} = \int_{\Omega_{\boldsymbol{\xi}}} \xi_1^{k_1} \xi_2^{k_2} \ldots \xi_{N_d}^{k_{N_d}} n(\boldsymbol{\xi}) \, \mathrm{d}\boldsymbol{\xi}. \tag{3.52}$$

A few methods to approach the problem of multivariate QBMM have been proposed so far. The most straightforward method was suggested by Wright et al. [97] and later referred to as "brute-force QMOM" by Marchisio and Fox [52]. The idea is very simple: A set of mixed moments defined as in Eq. 3.52 written in quadrature form (Eq. 3.31) constitutes a system of non-linear equations similar to Eq. 3.33. The solution of that system yields a multivariate quadrature approximation. However, there is no guarantee of convergence without a good initial guess. Other, rather complex multivariate inversion algorithms are the tensor-product QMOM, of which a general description can be found in Ref. [52], and the conditional QMOM (CQMOM) [99], which is based on conditional density functions.

A monokinetic assumption simplifies the moment inversion problem considerably. It means that all higher dimensions depend only on the first dimension (particle size), which corresponds to zero variance in the higher dimensions. It allows to express an N_d-dimensional NDF as

$$n(\xi_1, \xi_2, \ldots, \xi_{N_d}) = n(\xi_1) \cdot \prod_{i=2}^{N_d} n(\xi_i|\xi_1) \tag{3.53}$$

In terms of moments, this means that only the first order moments in higher dimensions are needed. Such an approach can be used in conjunction with the EQMOM (mk-EQMOM) assuming a functional dependence of higher dimenensions on the first dimension [23, 52].

A computationally efficient method for multivariate NDFs was developed as part of this work [66]. It is suitable specifically for problems where the monokinetic assumption is valid and where fluxes across the phase-space boundaries occur, which corresponds to the disappearance of droplets by vaporization ("zero-flux"). It uses a multivariate monokinetic EQMOM with beta or gamma KDFs to reconstruct the marginal NDF. Combined with a presumed functional dependence of $\xi_2 \ldots \xi_{N_d}$ on ξ_1 in terms of polynomials or splines, the proposed method allows closure of the moment transport equations related to multivariate PBEs with boundary-flux in phase space.

Although some methods exist for the application to multivariate NDFs, the extension to multiple dimensions can be considered one of the most problematic aspects of QBMM. In many cases, either the computational costs are prohibitive, the method lacks numerical stability or underlying assumptions are not justified for specific physical applications. Therefore, additional developments are required to make QBMM generally suitable for high-dimensional problems.

3.4.5 Moment Realizability

An important aspect of QBMM is moment realizability, which refers to the consistency of a moment set. A realizable set of moments is characterized by the existence of at least one valid density function. Otherwise, if the set is unrealizable, there is no density function corresponding to the given moments. A simple example of an unrealizable moment set is a set of which at least one moment of even order is negative. Based on the moment definition in Eq. 3.28, it is obvious that no non-negative NDF would yield such a set of moments.

While the moment set in the example above is easy to identify as unrealizable, it is conceivable that a set of only non-negative moments is inconsistent. Thus, a more accurate, mathematical definition of realizability shall be given, which is based on the work of Dette and Studden [18]: A set of N moments is realizable if it lies within the moment space M_N. The kth moment space M_k is always convex and k-dimensional. Figure 3.3 illustrates the second and third moment space related to a probability measure that is bounded on the interval $[0, 1]$.

Since the moment inversion algorithms described in the previous sections rely on valid moment sets, special care must be taken that realizability of the moment sets is preserved. Whether a set of moments is realizable, can be determined by related Hankel determinants [18, 25, 52]. More precisely, a moment set is realizable if the Hankel determinants

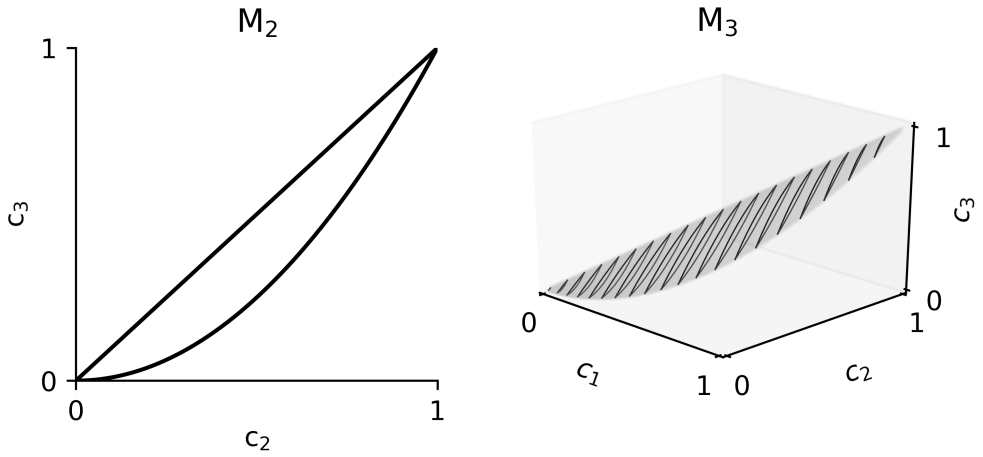

Figure 3.3: *The moment spaces M_2 (left) and M_3 (right) related to a probability measure bounded on the interval [0,1].*

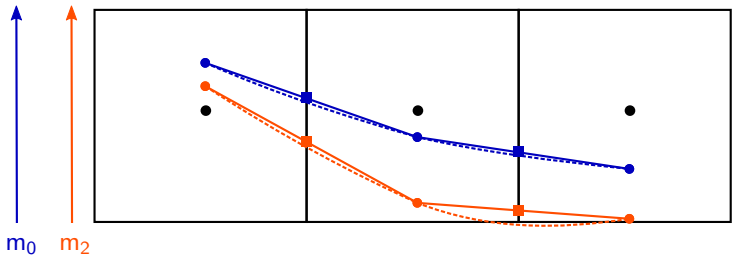

Figure 3.4: *Linear and higher-order interpolation of moments from the cell centers to the cell faces. Here, second-order interpolation results in an non-realizable moment set, due to an invalid second moment.*

$$\begin{vmatrix} c_k & c_{k+1} & \dots & c_{k+l} \\ c_{k+1} & c_{k+2} & \dots & c_{k+l+1} \\ \vdots & \vdots & \vdots & \vdots \\ c_{k+1} & c_{k+2} & \dots & c_{k+2l} \end{vmatrix} \geq 0 \qquad \forall \quad k \in \{0,1\}, \quad l \geq 0. \tag{3.54}$$

For cases where this condition is not satisfied, algorithms exist to correct an unrealizable moment set, e.g. the algorithms proposed by McGraw [53] and Wright [96]. However, correction algorithms modify the original set of moments, possibly to a significant extent. Thus, preventing the corruption of the original moment set should be preferred to the subsequent correction of invalid moments.

The most problematic step in the numerical procedure when solving a moment transport equation like Eq. 3.30 is the moment advection in physical space. Naturally, the typical numerical schemes do not ensure the consistency of moment sets. Only first-order schemes are guaranteed to preserve realizability, as a first-order scheme - given that the original moment set is realizable - corresponds to a weighted sum of valid moments, which again results in a realizable moment set. However, a first-order scheme is not the optimal choice, especially for moment transport, considering the strongly non-linear nature of moments (Eq. 3.28). The difficulty with higher order schemes is illustrated in Figure 3.4. Vikas et al. [90] developed higher-order advection schemes specifically for QBMM (see the original publication for a complete description). Essentially, not the moments directly but the quadrature nodes and weights are interpolated to the cell faces, which are subsequently used to construct the moments at the cell faces. As for the actual advection scheme, the time step size is limited based on a realizability criterion.

In this context, it is also worth mentioning that the moment transport equations generally need to be solved explicitly for the moment set to remain realizable, as moments may be corrupted due to the iterative procedure of implicit solution techniques. Evidently, the solution of moment transport equation is challenging. However, numerous novel methods and improvements have emerged from recent studies and the research is ongoing.

4 Modeling Spray Atomization

4.1 Physical Phenomena in Spray Systems

The evolution of a spray is governed by various interdependent processes. The general structure of a spray is illustrated in Figure 4.1, where the roman literals each indicate a physical process described below.

I Internal nozzle flow / cavitation.
The internal nozzle flow affects the spray formation significantly, as it determines the initial conditions. Depending on the nozzle geometry and the local flow conditions, cavitation may occur, which has strong effects on the conditions at the nozzle exit and primary atomization (cavitation-induced atomization).

II Primary atomization.
After a continuous liquid jet exits the nozzle, instabilities lead to disintegration of the core into smaller ligaments and drops. The perturbations can be caused by several phenomena, namely cavitation, shear-induced surface instabilities, turbulence and Rayleigh-instabilities, see Section 4.3.

III Secondary atomization.
Liquid structures formed as a result of primary breakup disintegrate further into smaller droplets until they reach a stable drop size. Various phenomena can cause fragmentation, depending on thermophysical properties of the droplets and local flow conditions. Possible drivers of secondary breakup are surface disturbances and - to a minor extent - gas-phase turbulence.

IV Vaporization.
If the spray is injected into hot gas a phase change from liquid to vapor takes place. Depending on the temperatures and pressures, flash-boiling may occur. However, under the conditions investigated as part of this thesis, the only phase-change mechanism is evaporation. Although all regions from the nozzle exit downstream are to some extent affected by evaporation, it can be considered to be the dominant phenomenon only in the dilute spray region, i.e. the region where no fragmentation processes occur.

Cavitation (I) is assumed to be absent in later investigations and is therefore not detailed any further. Evaporation of liquid droplets (IV) was addressed in Chapter 3. This chapter concentrates on the fragmentation processes, namely primary (II) and secondary breakup (III). These shall be discussed after a brief description of specific types of surface instabilities as possible drivers of breakup.

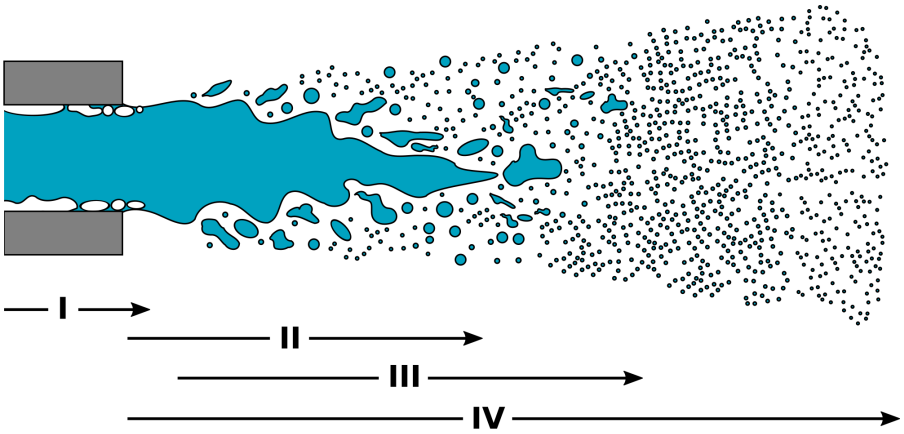

Figure 4.1: *The general structure of a liquid spray. Roman numerals indicate physical processes: (I) Internal nozzle flow / cavitation, (II) primary atomization, (III), secondary atomization, (IV) vaporization.*

4.2 Surface Instabilities

As mentioned in the previous section, the disintegration of a liquid jet or liquid droplets with a relative velocity to a surrounding gas can undergo breakup due to surface disturbances. This section is a brief introduction to the relevant types of surface instabilities. Essentially, three types of surface perturbations can cause breakup: (1) Kelvin-Helmholtz, (2) Rayleigh-Taylor and (3) Plateau-Rayleigh instabilities, which are schematically shown in Figure 4.2.

The Kelvin-Helmholtz (KH) instability is a shear induced surface instability that occurs in systems of two fluids with different densities and a velocity difference across the interface. The underlying theory was developed by Helmholtz [31] and Thomson [88] (Lord Kelvin). Essentially, KH instabilities describe the growth of surface waves induced by small disturbances in the (linear) tangential velocity. The interface becomes unstable exhibiting vortical structures. If the destabilizing waves exceed the stabilizing effect of surface tension, KH instabilities can eventually lead to disintegration. In the context of jet or drop breakup, this type of surface perturbation is particularly important in cases of relatively large interfacial areas subjected to high relative velocities. Detailed theoretical descriptions and analyses related to KH instabilities are given in [47, 55].

The second type of surface instabilities relevant in the context of liquid droplet breakup are the Rayleigh-Taylor (RT) instabilities, named after Rayleigh [71] and Taylor [84]. RT instabilities occur at the interface of two fluids with different densities where the lighter fluid is accelerating into the heavier one. The underlying theory of this phenomenon was derived by Rayleigh [71], showing that a system of two fluids with different densities with the heavy fluid over the lighter one is inherently unstable due to waves at the flat surface,

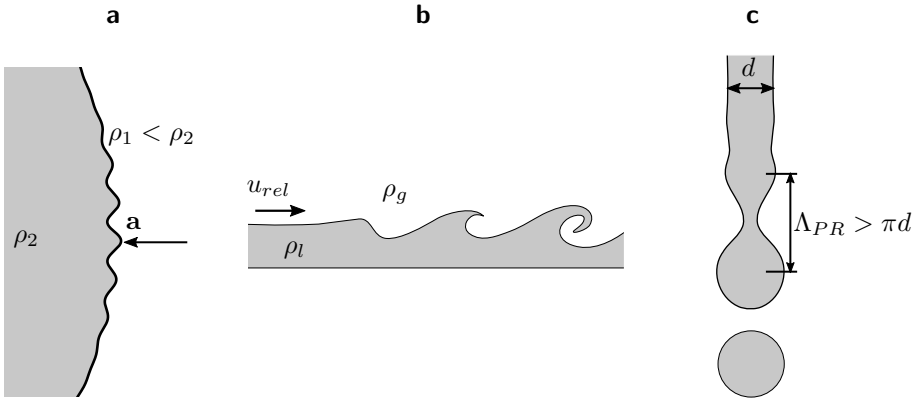

Figure 4.2: *Schmatic illustration of (a) Rayleigh-Taylor instabilities, (b) Kelvin-Helmholtz instabilities and (c) Plateau-Rayleigh instabilities.*

that grow exponentially with time. Decades later, Rayleigh's analysis was extended by Taylor [84] to a more general case of a two-fluid-system under an acceleration other than gravity perpendicular to the free surface towards the heavier fluid. Detailed descriptions of the theory of RT instabilities in general as well as RT-driven breakup are given in [41, 46, 81].

Plateau-Rayleigh instabilities, or simply Rayleigh instabilities, refer to the growth of small perturbations at the surface of a cylindrical liquid column. If the wavelength of the disturbances is sufficiently long, the increase in surface energy will cause a further progress of the surface wave growth [20], resulting in a local decrease of the jet diameter. Eventually, as the diameter in the pinch region tends to zero, a drop separates from the jet. Plateau's experimental investigations [64] indicated that the critical wavelength must be greater than the jet circumference for breakup to occur. This was later confirmed by Rayleigh's theoretical analysis [70]. The underlying physics of such disintegration processes are thoroughly analyzed in [19, 20].

4.3 Primary Atomization

Of the processes described in Section 4.1, primary atomization is of particular importance, as it determines the initial properties of the dispersed phase and thus initiates a chain of further processes leading to the formation of a fuel-air mixture. Despite its great significance, primary breakup has nonetheless remained one of the (if not the) most challenging components of a spray in terms of numerical modeling. In addition to the rather complex mechanisms controlling primary breakup, the lack of precise and reliable experimental techniques for optically dense sprays to produce reference data for model

validation further complicates the development of advanced models.

A number of different mechanisms can lead to disintegration of a liquid jet to produce secondary droplets. The types of primary breakup in the absence of cavitation are turbulence-induced breakup, shear-driven breakup and Rayleigh breakup. Turbulence-induced breakup refers to the disintegration of the jet as a result of collision with turbulent eddies, of which the energy is sufficiently high to overcome surface tension. Shear-driven breakup describes atomization due to shear forces and shear-induced surface perturbations such as KH instabilities. Rayleigh-breakup occurs as a consequence of growing Rayleigh-waves at the liquid surface. The dominant breakup mechanism is primarily determined by the jet Weber number with little dependence on the Reynolds number. The general tendency reported in studies on primary breakup [78, 98] is the following: At low Weber numbers, Rayleigh instabilities are dominant, while at higher Weber numbers there is a transition towards turbulence-induced atomization, and in the regime of very high Weber numbers ($\sim 10^5$) shear-driven breakup is the controlling mechanism.

4.3.1 Overview of Modeling Approaches

Numerous numerical models for the primary atomization of a liquid jet exist that are mainly distinguishable by

- how turbulence is modeled,
- how the presence and interaction of multiple phases is modeled,
- the fundamental assumptions which phenomena are critical with respect to jet disintegration.

The most accurate and straightforward method to simulate the turbulence-induced breakup of a liquid jet is DNS, where length scales as small as the Kolmogorov scale are resolved on the computational grid and hence no turbulence model is required. DNS has been used to investigate atomization of liquid jets in several studies, e.g. [17, 32, 48]. However, the applicability of DNS is limited to fundamental investigations of low-Reynolds and low-Weber number flows due to extremely high computational requirements (see Section 3.1). Consequently, DNS has no relevance for real engineering applications. LES is an affordable alternative for the detailed simulation of spray atomization (e.g. [2, 11]), though still accompanied by high numerical costs.

Turbulence models based on the RANS equations are the most practical models in terms of computational demands. However, RANS models lack the ability to capture turbulent flow structures. Therefore, additional atomization models are needed. Common models are based on the assumption that shear forces and KH instabilities rather than turbulence are the primary cause of atomization.

While in DNS and LES the liquid phase is often resolved on a particle scale using detailed interface models, RANS simulations are normally combined with LPT, representing the

liquid phase by discrete particles, as described in Section 3.3. Despite the availability of more sophisticated methods, the combination of a RANS turbulence model with LPT has remained prevalent for the simulation of sprays in real engineering applications, due to the simplicity and comparatively moderate numerical costs. A Lagrangian approach will be described in Section 4.3.2.

For flow configurations with a known dominant gradient direction such as boundary layer flows and jets, the one-dimensional turbulence (ODT) model [42] is an alternate approach to model turbulence by resolving all relevant length scales on a one-dimensional line of sight through a three-dimensional flow field. It combines high resolution on the 1D domain with moderate computational costs. ODT was recently applied to simulate the breakup of liquid jets, showing good agreement with experimental and DNS results [57, 58]. A description of the ODT model for primary breakup is given in Section 4.3.3.

4.3.2 The Lagrangian Blob Model

The blob injection method is an approach to model primary atomization of a liquid jet in a Lagrangian framework. It was first introduced by Reitz [72] and has been widely used in conjunction with LPT spray modeling ever since. Two essential assumptions are the basis of the originial model:

1. The behavior of a continuous liquid jet in terms of atomization can be approximated by spherical Lagrangian particles the size of the jet diameter.
2. Atomization is primarily controlled by KH instabilities.

The general procedure is as follows: Large drops, referred to as blobs, are added at the injection point with a predefined frequency and a diameter in the order of the nozzle hole. The mass results from the particle addition frequency and a given mass flow rate. The direction of the initial velocity vector is random within an angle that can be either a fixed specified value (e.g. based on measurements) or a result of theoretical considerations. The original model uses KH frequencies and wavelengths, though other correlations that include effects of turbulence, e.g. [38], are possible.

Immediately after injection, secondary drops are stripped off from the parent parcel by virtue of growing KH instabilities, which result from the so-called Wave-breakup model [72] (also referred to as KH model). The Wave-breakup model may also be considered a secondary breakup model. The used correlations will therefore be given in Section 4.4.2.2 (the KH equations). When the accumulated stripped off mass exceeds a defined threshold, which Reitz [72] chose to be 3 %, a child parcel is generated of which the size results from the KH wavelength. In this way, the number of child parcels is limited, which is necessary for computational reasons.

The approximation by spherical particles potentially results in excessive transfer of mass, heat and momentum due to the overestimated surface area compared to the actual jet.

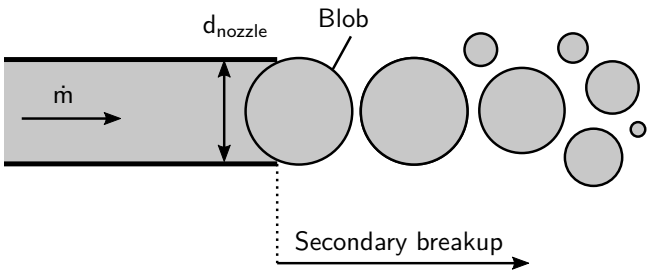

Figure 4.3: *Schematic illustration of the Lagrangian blob method based on Ref. [6].*

In most cases however, the time scales of atomization are sufficiently small to cause immediate breakup. A more substantial drawback of the model is a certain lack of predictive capability due to the sensitivity to its parameters. Nonetheless, the blob injection model has been employed in numerous studies on spray atomization, e.g. [7, 61], giving satisfactory results if the model parameters are chosen carefully.

4.3.3 The One-Dimensional Turbulence Model

In this section, a brief summary of the ODT model in the context of primary breakup modeling is given. Comprehensive descriptions of the ODT model and its extension and application to the breakup of turbulent liquid jets can be found elsewhere [42, 43, 58]. In contrast to the model outlined in the previous section, the core of the ODT atomization model is turbulence-induced breakup.

ODT is a stochastic model that approximates solutions to the governing transport equations of a 3D turbulent flow field, resolving the full range of relevant turbulent length scales on a 1D domain. The ODT domain is a notional line of sight through the 3D flow field, oriented in lateral direction with respect to the liquid jet and advected downstream with the liquid bulk velocity, see Fig. 4.4.

The essential feature of ODT is the modeling of turbulent advection through a stochastic sequence of instantaneous eddy events, characterized by the eddy location on the ODT line y_0 and size l. A mapping operation corresponding to each eddy event mimics the turbulence-induced increase of property gradients by implementation of the so-called triplet map. A triplet map takes a property profile within the spatial interval $[y_0, y_0 + l]$, compresses it to one-third of its original length, pastes three identical copies into the eddy range and reverses the middle copy to ensure continuity. In mathematical form, the post-eddy profile of a flow property ϕ along the ODT line can be expressed as

$$\hat{\phi}(y) = \phi(\hat{y}(y)), \tag{4.1}$$

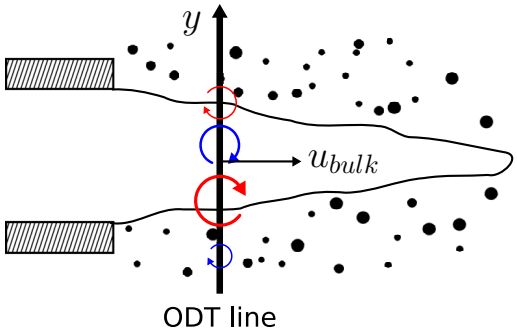

Figure 4.4: *Schematic representation of the ODT domain. Regular singlephase eddies are colored in blue, whereas the red eddies are multiphase eddies.*

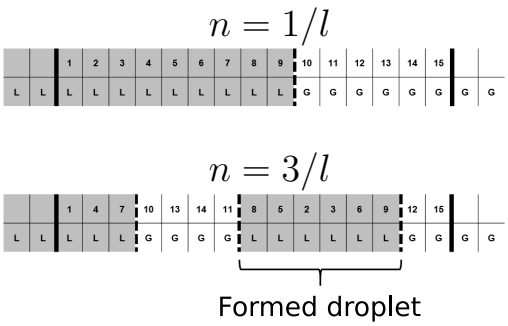

Figure 4.5: *Multiphase eddy treatment in ODT. The thick solid lines represent the eddy range. Interfaces between liquid (L) and gas (G) are represented by the dashed lines.*

where the mapping rule $\hat{y}(y)$ is defined as

$$\hat{y}(y) = y_0 + \begin{cases} 3(y-y_0), & \text{if } y_0 \le y \le y_0 + (1/3)l, \\ 2l - 3(y-y_0), & \text{if } y_0 + (1/3)l \le y \le y_0 + (2/3)l, \\ 3(y-y_0) - 2l, & \text{if } y_0 + (2/3)l \le y \le y_0 + l, \\ y - y_0, & \text{otherwise.} \end{cases} \tag{4.2}$$

The triplet map is measure preserving, which means that all integral properties are identical before and after the mapping operation. The presented formulation of the triplet map is equivalent to a relocation of a fluid parcel from $\hat{y}$ to y. Thus, advancement of the velocity profile requires additional operations which take into account the redistribution of energy among the velocity components due to pressure gradients, surface tension forces and other energy-conversion processes. In the presence of such phenomena the velocity profile is updated according to

$$\hat{u}_i(y) = u_i(\hat{y}(y)) + c_i K(y) + b_i J(y), \tag{4.3}$$

where $K(y) = y - f(y)$ and $J(y) = \big|K(y)\big|$ are kernel functions enabling the exchange of kinetic energy between the velocity components while satisfying the conservation of total energy. The only unknowns in Eq. 4.3 that must be found through modeling are the coeffients c_i, since b_i and c_i have a specified functional dependence. The determination of c_i is based on energy conservation and general considerations on the properties of turbulent flow, described in detail by Ashurst and Kerstein [3, 4].

Eddy events are individually parameterized by position l and size y_0, sampled from an instantaneous distribution that evolves with the flow. The number of events during a time increment dt for eddies located within $[y_0, y_0 + dy]$ in the size range $[l, l + dl]$ is denoted $\lambda(y_0, l; t)dy_0 dl dt$, where the event rate density λ is defined as

$$\lambda(y_0, l; t) = C/(l^2 \tau(y_0, l; t)). \tag{4.4}$$

The adjustable parameter C scales the overall eddy frequency and τ is the eddy time scale, which is found by

$$(l/\tau)^2 \sim E_{final} - Z(\nu^2/l^2), \tag{4.5}$$

where E_{final} is the final value of the available energy, which is equal to the kinetic energy E_{kin} in the absence of phase interfaces. Z is a parameter suppressing unphysical eddies smaller than the Kolmogorov length scale. As the computational costs to reconstruct the distribution for every eddy event or advancement of Eq. 4.3 would be prohibitive, an equivalent Monte-Carlo method called thinning [75] is employed.

In ODT, the jet is represented as a contiguous liquid region on some interval $[y_1, y_2]$. A multiphase eddy contains at least one interface, i.e. its range $[y_0, y_0 + l]$ encloses one or both of the limits y_1 and y_2, see the red eddies in Fig. 4.4. Such cases require consideration of the change in surface tension energy ΔE_σ by virtue of droplet formation. Thus, in the presence of at least one phase interface, the available energy in Eq. 4.5 must satisfy

$$E_{final} = E_{kin} - \Delta E_\sigma. \tag{4.6}$$

The total surface tension energy density can be written as

$$E_\sigma = \frac{\sigma\alpha}{\overline{\rho}}, \tag{4.7}$$

where σ, α and $\overline{\rho}$ are the suface tension, the surface area per unit volume and the mean density, respectively. On the ODT domain, interfaces are in the form of isolated points. Thus, the increase of interfacial area must be found by geometric interpretation. Here, it is assumed that the interface is a statistically homogeneous isotropic random surface [57]. In this case, geometric analysis [12] shows that

$$\alpha = 2n, \tag{4.8}$$

where n is the number density of interface intersections. Since there are exactly two interfaces on the ODT domain, n can be 0, $1/l$ or $2/l$, corresponding to the number of interfaces within the eddy range. Fig. 4.5 illustrates, how triplet mapping as a permutation of cells triples the interface and produces three interfaces to form a new droplet. This can also be interpreted as a tripling of interfacial area. Consequently, the post-eddy number density can be $n = 0$, $3/l$ or $6/l$. Based on these considerations as well as Eq. 4.7 and Eq. 4.8, the change in surface tension energy can be expressed as

$$\Delta E_\sigma = \frac{2\sigma\Delta n}{\overline{\rho}}, \tag{4.9}$$

where Δn can attain values of 0, $2/l$ or $4/l$ corresponding to zero, one or two interfaces, respectively.

Besides the essential feature of the ODT model, which is turbulence-induced atomization, Rayleigh breakup and shear-driven breakup were considered as additional jet disintegration mechanisms in the model formulation. Details are provided in Ref. [58].

For the sake of clarity and completeness, it should be emphasized that ODT as an atomization model in its current form is applicable to statistically stationary jets. Transient jet development is not represented. A numerical investigation using a combination of ODT and LPT to simulate a full gasoline spray was carried out in *Publication I*.

4.4 Secondary Atomization

4.4.1 Atomization Regimes

The second type of atomization is the secondary breakup of droplets. That is, liquid structures and droplets larger than a stable size, which is determined by thermophysical particle properties and local flow conditions, disintegrate into smaller droplets until inertial forces are no longer sufficient to overcome surface tension forces. The secondary breakup behavior is thus primarily characterized by the drop Weber number. In terms of numerical modeling, secondary breakup is less problematic than primary breakup, as jet breakup can be viewed as a transfer of liquid from a continuous phase to the dispersed phase, whereas droplet breakup occurs only in the dispersed phase.

A considerable number of studies on the fragmentation of drops have been published during the last decades, many of which focused on the identification and quantification of different breakup modes. Figure 4.6 illustrates the drop breakup regimes reported by different authors, depending on the Weber number. Considering the use of various terms for identical breakup morphologies, five distinct modes of liquid drop breakup exist, namely (1) vibrational breakup, (2) bag breakup, (3) multimode breakup, (4) shear breakup and (5) catastrophic breakup.

Vibrational breakup refers to the fragmentation of a drop in the absence of aerodynamic forces. This type of breakup is driven solely by oscillations of the drop at is natural frequency due to surface tension. Since this mechanism is very slow and the resulting fragment sizes are large, it is commonly ignored [30].

Bag breakup occurs in a range of Weber numbers greater than ∼11, That value or a similar one is consistently reported in the literature. However, it may vary due to viscous effects of which the significance is expressed in terms of the Ohnesorge number. An empirical correlation for the dependence of the critical Weber number, where bag breakup is initiated, was first given by Brodkey [9]:

$$We_c = 10.96(1 + 1.077Oh^{1.64}). \tag{4.10}$$

Other authors derived similar expressions with slightly different constants. When $Oh \lesssim 0.1$ the effect of viscosity can be considered negligible and the onset of breakup independent of Oh.

Bag breakup is always initiated by a deformation, increasing the surface area perpendicular to the dominant flow direction, until a bag-like structure is formed. Subsequently, the

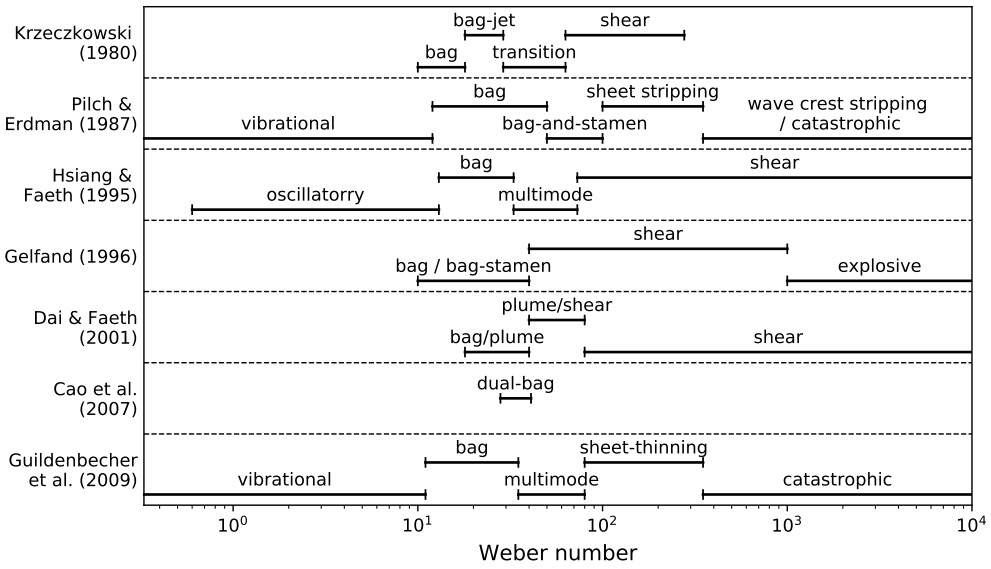

Figure 4.6: *Breakup regimes at low Ohnesorge numbers identified in different studies of Krzeczkowski [44], Pilch and Erdman [63], Hsiang and Faeth [36], Gelfand [26], Dai and Faeth [16], Cao et al. [10], Guildenbecher et al. [30].*

first breakup of the bag results in the formation of a toroidal ring and small fragments of almost uniform size. The ring then disintegrates into smaller droplets, which have been observed to be considerably larger than the children drops of the first breakup of the bag. The volume fractions of the bag and ring as well as the droplet sizes after breakup were determined experimentally by Chou and Faeth [13]. The two-stage breakup implies a multimodal fragment size distribution, although Hsiang and Faeth [34] found that a universal root normal distribution with MMD/SMD[1] ≈ 1.2 fits the size distribution after disintegration reasonably well. However, Guildenbecher et al. [29] conducted a detailed experimental study including drop size measurements and found a multimodal distribution, albeit with an MMD-to-SMD ratio of approximately 1.2.

The large surface area perpendicular to the flow suggests that RT-instabilities play a major role in the bag breakup regime. This is supported by experimental, numerical and theoretical studies [40, 45, 85, 87, 102, 103]. As vibrational breakup is commonly neglected, the onset of bag breakup is considered the first criticality with respect to secondary atomization [30, 85].

The *multimode breakup* regime refers to the transition from bag to shear breakup. Different breakup morphologies were identified, such as "bag-and-stamen" [63], "dual-bag breakup" [10] or "bag/plume" and "plume-shear" [16]. It is assumed that the physi-

[1]The MMD is the mass median diameter, SMD the Sauter mean diameter.

cal mechanisms as well as the morphologies are some combination of bag and shear breakup [30].

The *shear breakup* mode is associated with high Weber numbers. It is characterized by a sheet that is stripped from the periphery of the deformed droplet and breaks up into smaller droplets, while the coherent core drop remains until after disintegration. The size of the product droplets were found to correspond to MMD/SMD ≈ 1.2 by several authors [14, 15, 29, 35]. In Figure 4.6 shear breakup is also referred to as sheet stripping and sheet thinning. Whether the stripping mechanism due to viscous forces or the thinning mechanism due to aerodynamic forces controls the breakup process is a subject of disagreement among researchers [30]. Theofanous and colleagues [85, 87] concluded from experimental and numerical studies as well as theoretical considerations that KH-instabilities are the primary cause of this type of atomization.

Catastrophic breakup is attributed to large-amplitude surface waves that penetrate a drop and initiate a cascading process in which fragments can undergo multiple consecutive breakups [63]. Here, catastrophic breakup is assumed to be irrelevant in sprays because of the high Weber number range where it occurs. Theofanous and Li [86] suggest that obeservations of catastrophic breakup are only based on measurement artifacts and that a catastrophic breakup mode does not exist.

In conclusion, despite the fact that many studies on drop fragmentation have been published, the physical mechanisms that control droplet disintegration in different regimes are not completely understood. However, based on the brief review above, the following three breakup modes are generally presumed present in sprays: (1) bag breakup, (2) shear breakup and (3) multimode breakup which is a transitional mode between (1) and (2).

4.4.2 Lagrangian Breakup Modeling

4.4.2.1 The Model of Reitz and Diwakar

An early model for the secondary atomization of liquid drops in the context of engine-like sprays was proposed by Reitz and Diwakar [73, 74]. Based on the breakup regimes and limits identified by Nicholls [59], they formulated a model for bag breakup and shear breakup[2].

The lifetimes of unstable drops are given as

$$\tau_b = C_{\tau,b}\sqrt{\frac{\rho_d r_d^3}{\sigma}}, \tag{4.11}$$

$$\tau_s = C_{\tau,s}\frac{r_d}{u_r}\sqrt{\frac{\rho_d}{\rho_c}} \tag{4.12}$$

[2]In the orignial publication the breakup mode is referred to as "stripping breakup". Here, the term "shear" breakup is used for the sake of consistency with earlier sections.

for the bag and shear breakup regime, respectively. The constants $C_{\tau,b}$ and $C_{\tau,s}$ are of order unity. Here, the droplet size is given in terms of radius r_d. Accordingly, the first criticality, i.e. the onset of bag breakup, is determined by

$$We_r \geq C_{c,b} = 6, \tag{4.13}$$

where We_r is the radius-based Weber number. Hence, the first criticality in terms of diameter agrees with the observations reviewed in Section 4.4.1. In case of Eq. 4.13 being true, bag breakup takes place only if the condition for shear breakup defined as

$$\frac{We_r}{\sqrt{Re}} \geq C_{c,s} = 0.5, \tag{4.14}$$

is not satisfied. It should be noted that, while the bag breakup condition is commonly used, the Reynolds-number dependence in the shear breakup condition is somewhat contradictory to most of the experimental studies on secondary atomization.

Due to a lack of information on the daughter drop size distribution, they assumed a uniform stable radius of fragments r_c equal to the size that corresponds to the onset of breakup, assuming constant ambient conditions. In other words, they chose r_c to exactly match Eq. 4.13 or Eq. 4.14 in the respective regime. The temporal evolution of the particle size is then governed by the rate equation

$$\frac{\mathrm{d}r}{\mathrm{d}t} = \frac{r_c - r}{\tau}, \tag{4.15}$$

which is usually solved implicitly.

4.4.2.2 The Kelvin-Helmholtz/Rayleigh-Taylor Model

A well-established and one of the most frequently used models for secondary atomization in spray applications is the hybrid Kelvin-Helmholtz/Rayleigh-Taylor (KH-RT) breakup model [7, 61], which is built upon the ideas and developments of Reitz and Diwakar [73], Reitz [72] and Su et al. [83]. It is based on the assumption that drop breakup is initiated by a combination of simultaneously growing surface perturbations due to KH- and RT-instabilities. The two instabilities act as competing mechanisms with the faster one eventually leading to fragmentation.

The equations describing the growth of KH surface waves were derived by Reitz [72]. The two relevant quantities in terms of drop fragmentation are the frequency of the fastest-growing wave

$$\Omega_{KH} = \frac{0.34 + 0.38We_r^{1.5}}{(1 + Oh_r)(1 + 1.4Ta_r^{0.6})} \sqrt{\frac{\sigma}{\rho_d r_d^3}} \tag{4.16}$$

and its corresponding wavelength

$$\Lambda_{KH} = \frac{9.02 r_d (1 + 0.45\sqrt{Oh_r})(1 + 0.4Ta_r^{0.7})}{(1 + 0.867We_r^{1.67})^{0.6}}, \tag{4.17}$$

where the subscript r denotes a definition based on radius. $Ta_r = Oh_r\sqrt{We_r}$ is the Taylor number. The drop lifetime in the presence of growing KH-instabilities is defined as

$$\tau_{KH} = \frac{3.726 B_1 r_d}{\Omega_{KH}\Lambda_{KH}}, \tag{4.18}$$

where B_1 is a constant that has been chosen from a wide range of values between 10 and 60 [7]. The product droplets of KH-breakup are determined based on the wavelength of the fastest-growing wave, i.e.

$$r_{c,KH} = B_0\Lambda_{KH}, \tag{4.19}$$

where B_0 is a constant equal to 0.61. As the model was developed specifically for a Lagrangian representation of the dispersed phase, a restriction of the number of generated child parcels is essential for the application to real physical problems. This was considered in the model formulation by combination of the rate equation (Eq. 4.15) for droplet size with a limitation of the child parcels, such that a child is only generated if the accumulated mass stripped off the parent parcel, which follows from Eq. 4.15, exceeds a defined threshold, e.g. 3 % as in the original model.

The breakup of droplets due to RT-instabilities is treated in a similar way. The rate of the fastest growing wave is

$$\Omega_{RT} = \sqrt{\frac{2}{3\sqrt{3\sigma}}\frac{(-g_t\Delta\rho)^{3/2}}{\Sigma\rho}} \tag{4.20}$$

and the corresponding wave number

$$K_{RT} = \sqrt{\frac{-g_t\Delta\rho}{3\sigma}}, \tag{4.21}$$

where g_t is the droplet acceleration (Eq. 3.22) along the droplet trajectory. The lifetime of a droplet perturbed by surface waves of the RT-type is then

$$\tau_{RT} = \frac{C_\tau}{\Omega_{RT}}, \tag{4.22}$$

where C_τ is a constant of order unity. Analogous to the KH breakup, the product drops of RT-breakup are proportional to the wavelength of the fastest growing wave, i.e.

$$r_{c,RT} = \frac{\pi C_{RT}}{K_{RT}}. \tag{4.23}$$

where C_RT is another constant of order unity. With respect to the Lagrangian modeling approach, atomization due to RT-instabilities is implemented as follows. If the wavelength of the fastest-growing surface wave is smaller than the droplet diameter (since only such waves can break a droplet), the wave is tracked by incrementing a characteristic particle breakup time, until that time exceeds the droplet lifetime (Eq. 4.22). The droplet then disintegrates into equally sized fragments (Eq. 4.23). Moreover, the RT-breakup is prioritized, i.e. KH-breakup only occurs if RT-instabilities are not suffieciently large to cause drop breakup. A complete description of the algorithm is given by Patterson and Reitz [61].

4.4.3 QBMM Breakup Modeling

Up to here, the source term in the PBE due to discontinuous events $\mathcal{Q}_\xi$ (Eq. 2.28) and its moment transform $\mathcal{Q}_{c,k}$ (Eq. 3.30) were assumed to be equal to zero. In this section, the source term formulation for QBMM in the presence of breakup for a univariate PBE shall be given. Presuming the absence of aggregation/coalescence, the source term Eq. 2.28 is

$$\mathcal{Q}_\xi = \int_\xi^\infty \nu(\xi')\beta(\xi|\xi')n(\xi')\,\mathrm{d}\xi' - \nu(\xi)n(\xi), \tag{4.24}$$

where ξ' and $\nu(\xi)$ denote the parent drop size and the breakup frequency, respectively. The function $\beta(\xi|\xi')$ is the conditional daughter distribution of ξ given ξ'. The first term on the RHS is the birth term accounting for the generation of new particles as a result of fragmentation. The second term on the RHS represents the disappearance of particles. Applying the moment transformation yields the source term in the moment equation

$$\mathcal{Q}_{c,k} = \int_0^\infty \xi^k \int_\xi^\infty \nu(\xi')\beta(\xi|\xi')n(\xi')\,\mathrm{d}\xi'\,\mathrm{d}\xi - \int_0^\infty \xi^k\nu(\xi)n(\xi)\,\mathrm{d}\xi. \tag{4.25}$$

This can can also be written as [52, 68]

$$\mathcal{Q}_{c,k} = \int_0^\infty \nu(\xi')n(\xi') \int_0^{\xi'} \xi^k\beta(\xi|\xi')\,\mathrm{d}\xi\,\mathrm{d}\xi' - \int_0^\infty \xi^k\nu(\xi)n(\xi)\,\mathrm{d}\xi \tag{4.26}$$

Using an N_α-point Gaussian quadrature, the source term in the moment equation is thus

$$\mathcal{Q}_{c,k} = \sum_{\alpha=1}^{N_\alpha} \left[\int_0^{\xi_\alpha} \xi^k\beta(\xi|\xi')\,\mathrm{d}\xi - \xi_\alpha^k\right] \nu(\xi_\alpha)w_\alpha. \tag{4.27}$$

The corresponding expression for an EQMOM approach only contains an additional inner sum over the $N_{\alpha,\beta}$ second quadrature nodes.

Numerous breakup kernels have been developed for PBEs. The advantage of population balance models with respect to breakup is that there is no restriction to the daughter size distribution. Therefore, it is possible to develop models with a more profound physical basis. A comprehensive overview of proposed breakup rate formulations and daughter size distributions is given in the review article of Liao and Lucas [49]. However, the known models related to PBEs are - though usually not explicitly stated - almost exclusively suitable for bubble flows, since they assume collisions with turbulent eddies in the continuous phase to be the primary mechanism of fragmentation. This is not necessarily true for sprays with a fundamentally different density ratio, where surface instabilities dominate breakup. Additionally, the models were not formulated for QBMM, and many are not directly applicable, since the integral term in Eq. 4.27 may not be analytically solvable. Thus, further developments in the field of breakup models specifically for liquid droplets in the QBMM context are needed.

As a very simple, yet well-established spray breakup model the model of Reitz and Diwakar, which was presented in Section 4.4.2.1, shall be derived for QBMM here. It was

originally designed as a Lagrangian model and has - to the author's best knowledge - only been applied as such. Here, the rate equation given in Eq.4.15 is omitted for the following reason: Since the Lagrangian approach is subject to computational restrictions in terms of the number of child parcels, such an expression may be required in that case. However, it corresponds to a continuous decrease in droplet size and disregards the discontinuous nature of a fragmentation process. Moreover, no variance is introduced to a monodisperse system (or single droplet), which is in contradiction to experimental observations and theoretical considerations. Population balance models are not limited in that way. Thus, the discontinuous atomization process can be treated as such.

Let the internal coordinate be $\xi = d = 2r_d$. Moreover, the constants $C^*_{c,b}$ and $C^*_{c,s}$ are introduced, corresponding to $C_{c,b}$ and $C_{c,s}$ on a diameter-basis. Taking into account the definitions of the Weber and Reynolds number, the breakup limits in Eq. 4.13 and Eq. 4.14 can be expressed in terms of the critical droplet sizes

$$\xi_{c,b} = C^*_{c,b}\frac{\sigma}{\rho_c \Delta u^2}, \tag{4.28}$$

$$\xi_{c,s} = C^{*^2}_{c,s}\frac{\sigma^2}{\rho_c \mu_c \Delta u^3}, \tag{4.29}$$

where Δu denotes the relative velocity magnitude. The monodisperse daughter distribution is merely a Dirac Delta function located at the critical particle size (see Section 4.4.2.1). Introducing the subscript m, which can be either b or s, to indicate the breakup mode, the daughter size distribution is defined as

$$\beta_m(\xi|\xi') = \left(\frac{\xi'}{\xi}\right)^3 \delta\left(\xi - \xi_{c,m}\right). \tag{4.30}$$

The factor $(\xi'/\xi)^3$ follows from mass conservation. The rates for bag breakup and shear breakup are equal to τ_b^{-1} (Eq. 4.11) and τ_s^{-1} (Eq. 4.12), respectively. Consequently, the breakup frequencies are determined by

$$\nu_b(\xi) = H(\xi - \xi_{c,b})\left[1 - H(\xi - \xi_{c,s})\right]\frac{1}{C_{\tau,b}}\sqrt{\frac{\sigma}{\rho_c}}\xi^{-3/2}, \tag{4.31}$$

$$\nu_s(\xi) = H(\xi - \xi_{c,s})\frac{1}{C_{\tau,s}}\sqrt{\frac{\rho_c}{\rho_d}}\Delta u \xi^{-1}, \tag{4.32}$$

where H denotes the Heaviside step function, taking into account the breakup limits given in Section 4.4.2.1. The definition

$$\nu(\xi)\beta(\xi|\xi') = \nu_b(\xi)\beta_b(\xi|\xi') + \nu_s(\xi)\beta_s(\xi|\xi') \tag{4.33}$$

and substitution into Eq. 4.27 yields the final expression for Reitz-Diwakar breakup

$$\begin{aligned}\mathcal{Q}_{c,k} = \sum_{\alpha=1}^{N_\alpha} H(\xi_\alpha - \xi_{c,b}) w_\alpha \cdot \Bigg[& [1 - H(\xi_\alpha - \xi_{c,s})]\frac{1}{C_{\tau,b}}\sqrt{\frac{\sigma}{\rho_c}}\xi_{b,s}^{k-3}\xi_\alpha^{3/2} \\ & + H(\xi_\alpha - \xi_{c,s})\frac{1}{C_{\tau,s}}\sqrt{\frac{\rho_c}{\rho_d}}\xi_{c,s}^{k-3}\xi_\alpha^{k-1}\Bigg].\end{aligned} \tag{4.34}$$

This expression is validated in Section 5.3 by application to a quasi-zero-dimensional test case in combination with EQMOM.

5 Results and Discussion

5.1 Simulations of a Gasoline Spray

5.1.1 ECN Spray G

The Engine Combustion Network (ECN) is a collaboration among researchers in engine combustion. It provides several reference sprays, one of which is Spray G that is numerically studied in the next sections.

Spray G is a gasoline spray injected with a pressure of 200 bar through an eight-hole nozzle. It is evaporating and non-reacting under the standard operating conditions (Spray G1). The nominal operating parameters are given in Table 5.1. The nozzle geometry is depicted in Figure 5.1.

Table 5.1: Nominal operating parameters of the ECN Spray G

Ambient gas temperature	300 °C (573 K)
Ambient gas density	3.5 kg/m^3
Fuel	Iso-octane
No. of nozzle holes	8
Injection pressure	20 MPa (200 bar)
Injected liquid mass	10 mg
Fuel temperature	363 K
Nozzle diameter	165 μm
Injection duration	780 μs

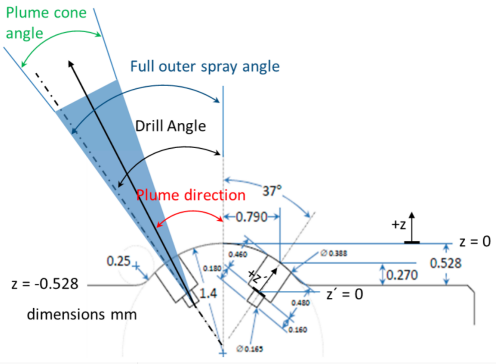

Figure 5.1: *Specified nozzle geometry of the ECN Spray G [21].*

5.1.2 Eulerian-Lagrangian Simulation

With Spray G as a well-documented reference case, a numerical investigation was carried out. A standard RANS approach was used to account for gas phase turbulence. That is, the Eqs. 3.5 - 3.8 were solved numerically with an operator splitting based on the PISO (Pressure-Implicit with Splitting of Operators) algorithm [39]. The related computational mesh is depicted in Figure 5.2. It is refined in all directions in the nozzle region. The Lagrangian submodels that were employed are given in Table 5.2.

Table 5.2: Submodels applied to Lagrangian spray parcels

Drag	Dynamic droplet drag
Evaporation	Spalding mass transfer coefficient and Ranz-Marshall correlation
Heat transfer	Ranz-Marshall correlation
Turbulent dispersion	Stochastic dispersion with a Gaussian distribution [1]
Injection model	Blob injection
Primary breakup	KH-RT [72]
Secondary breakup	KH-RT [72]

Figure 5.3 shows the penetration lengths of liquid and vapor defined as the distance from the nozzle along the vertical axis where the volume fraction (liquid) or mass fraction (vapor) exceeds the threshold of 0.1 %. Both reproduce the experimentally determined penetration reasonably well. The fluctuations result from the post-processing method, where the center of a cell exceeding the defined threshold was taken as the penetration length, without interpolation.

It should be noted that results of different experimental studies for the liquid penetration during the period after the end of injection vary significantly [51], which is mainly caused by different methods of image processing rather than actual physics, and the thresholds defined in the context of optical measurements do presumably not correspond to 0.1 % volume fraction. Hence, detailed comparisons in the very dilute spray region can be considered meaningless.

5.1.3 ODT-LPT Simulation

Another numerical study was conducted on Spray G, using the ODT model for primary atomization. The results of the ODT simulation in terms of the local jet diameter, local drop size distributions and velocities were utilized to predefine the primary breakup in an Eulerian-Lagrangian simulation. Except for the ODT primary breakup model, the numerical setup was similar to the one presented in the previous section, though only a single spray plume was considered, i.e. the domain was only a 45-degrees sector of the

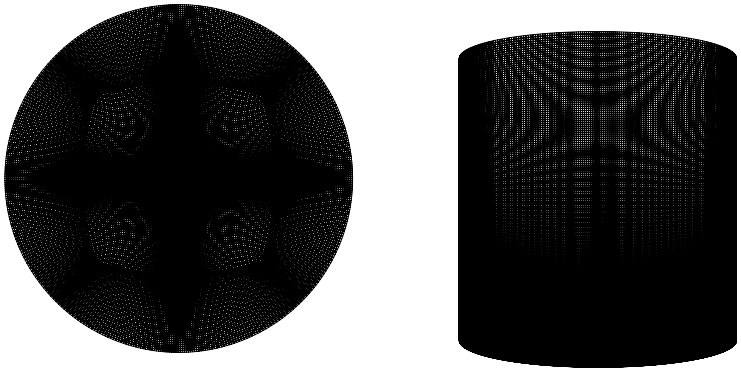

Figure 5.2: *Computational grid for the Eulerian-Lagrangian simulation of Spray G*

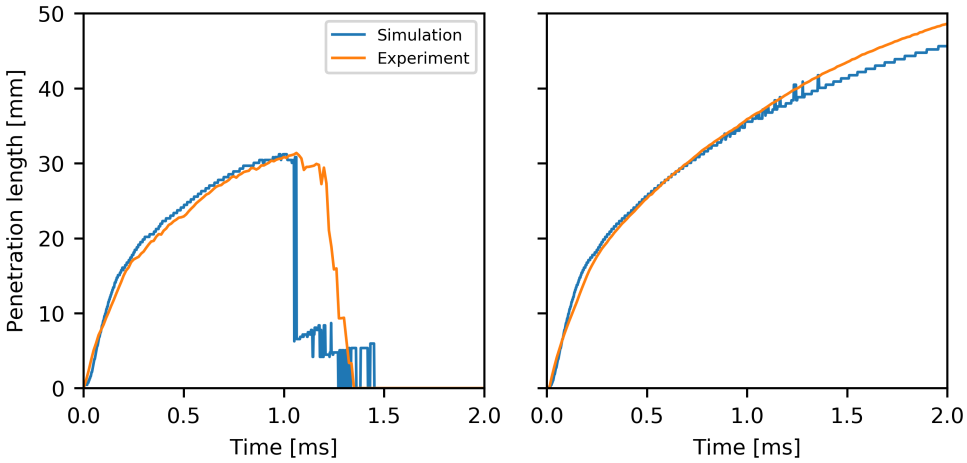

Figure 5.3: *Spray penetration lengths from Eulerian-Lagrangian simulation compared with experimental data of Manin et al. [51]*

cylinder. A more detailed description of the coupling method and the numerical setup is given in *Publication I*.

Figure 5.4 shows a visualization of the Lagrangian particles forming the spray plume. It illustrates how small droplets, of which the properties were determined by the ODT simulations, separate from the liquid core that is represented by large particles in the Euler-Lagrange simulation.

The penetration lengths of liquid and vapor, defined as stated in the previous section,

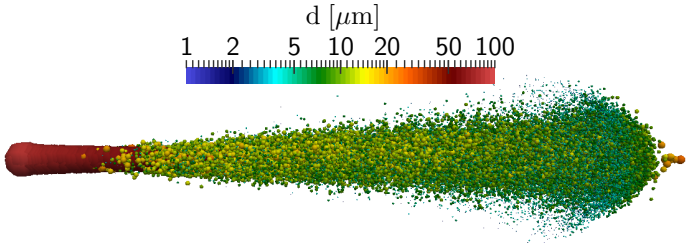

Figure 5.4: *Visualization of the spray plume from a ODT-LPT simulation*

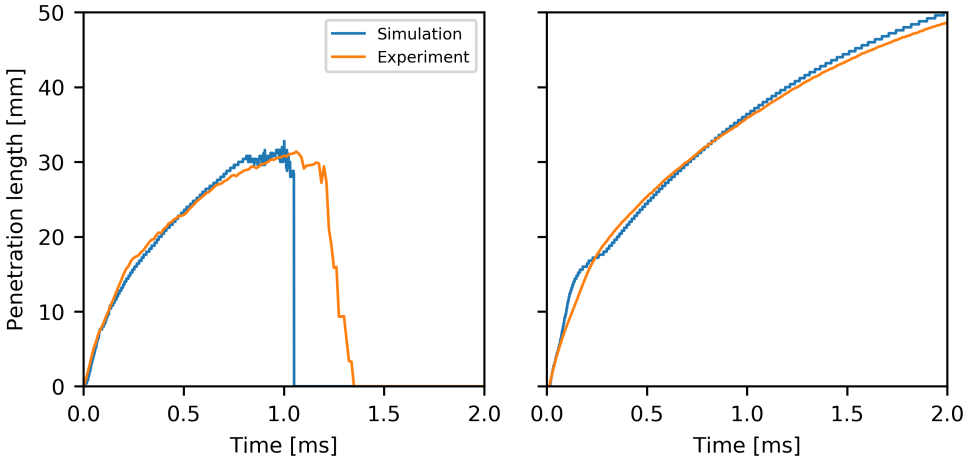

Figure 5.5: *Spray penetration lengths from ODT-LPT simulation compared with the experimental data of Manin et al. [51]*

are depicted in Figure 5.5. The results indicate that the ODT model may serve as a suitable alternative that requires less tuning compared to conventional Lagrangian primary breakup models such as the KH-RT/blob model. However, additional modeling efforts are required to adjust the ODT model to transient jet development. The limitation of ODT to statistically stationary jets becomes apparent particularly in the vapor penetration during the initial transient injection phase. More results and discussions can be found in *Publication I*.

5.2 One-Dimensional QBMM Validation

In this section, results of coupled EQMOM-CFD simulations with a relatively simple numerical setup are presented and discussed. The investigated case is the injection of droplets into a hot surrounding gas, considering a one-dimensional motion, heating and evaporation. The conditions in terms of temperatures, pressure and the type of fuel are identical to the Spray G conditions. The setup is schematically illustrated in Figure 5.6.

The initial distribution was chosen to be of a Rosin-Rammler shape, which is a typical distribution in fuel sprays. The volume-based probability density function (PDF) is defined as

$$f(\xi) = \frac{\theta}{\bar{\xi}} \left(\frac{\xi}{\bar{\xi}} \right)^{\theta-1} e^{-(\xi/\bar{\xi})^{\theta}}, \tag{5.1}$$

where the parameters were chosen to be $\theta = 2.1$ and $\bar{\xi} = 50$ μm. In the reference simulation, a high-resolution LPT simulation, particles that are injected with a frequency of 10^6 s^{-1} are sampled from the given distribution. This number was determined in a pre-investigation on the convergence of LPT results with respect to the parcel injection frequency. The moments for the EQMOM computation were obtained by numerical integration, as Eq. 5.1 transformed to a number basis is not analytically integrable. Injection occurs through a moment flux across the inlet boundary.

A univariate EQMOM with two KDFs and four second quadrature nodes per KDF was employed, i.e. the only internal coordinate is the diameter $\xi = d$. The drop velocity, which is equivalent to the advection velocity in the moment equations, as well as the drop temperature are only accounted for in terms of mean values. For that purpose, additional transport equations for drop velocity and temperature are solved.

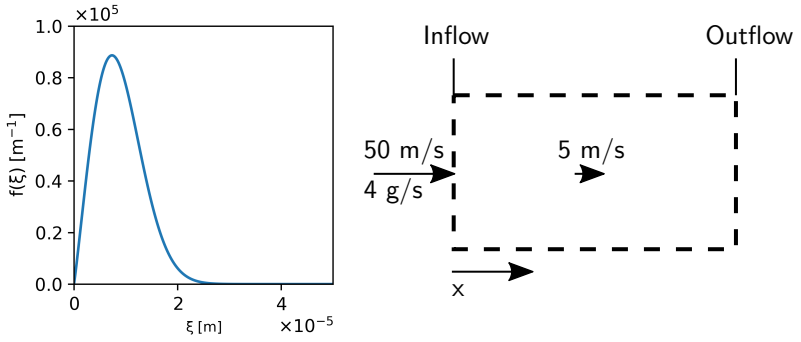

Figure 5.6: *Schematic illustration of the case setup*

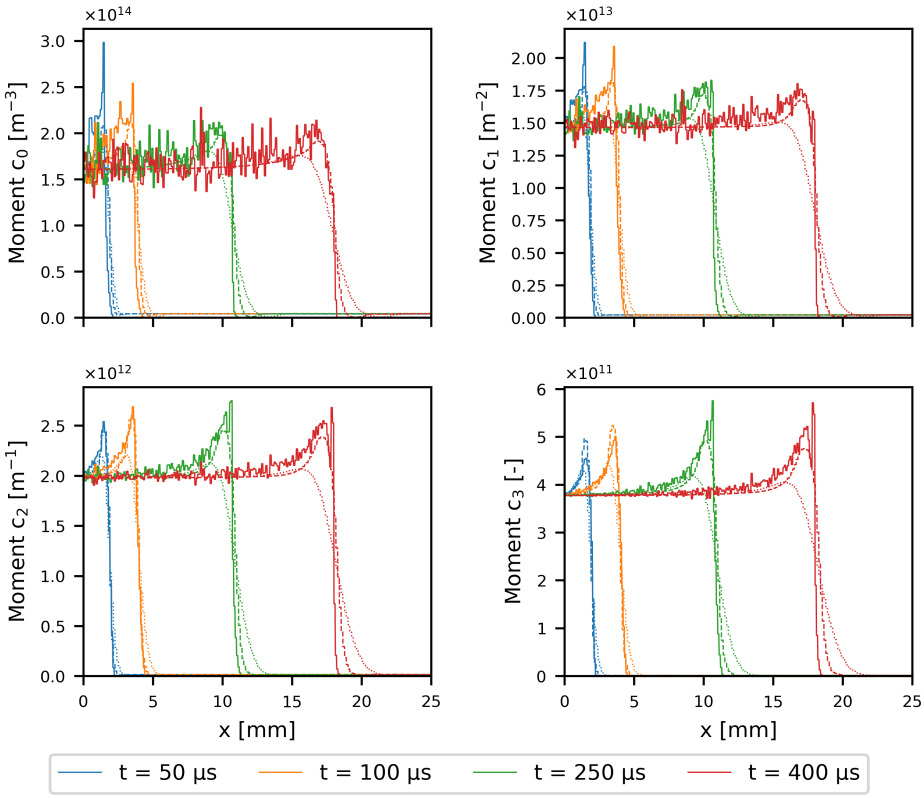

Figure 5.7: *Comparison of an EQMOM simulation with an Eulerian-Lagrangian simulation in terms of moments up to the third order. The solid lines represent the Lagrangian simulation, the dotted line EQMOM with a first-order advection scheme and the dashed line EQMOM with a second-order advection scheme.*

The moments up to third order are shown in Figure 5.7, where the solid lines represent the reference results from the LPT simulation. The dotted and dashed lines represent the moments from EQMOM-CFD simulations with a first-order and second-order discretization of the moment advection in physical space, respectively. They agree relatively well with the reference solution. The first-order scheme however fails to capture the peak at the spray front. Since the peak does not change considerably over time, the differences are most likely attributed to the steep moment gradient at the start of injection where higher-order schemes are particularly advantageous. A temporal second-order discretization and second-order advection in phase space were also applied in additional calculations but did not exhibit any similar effects.

The changes in iso-octane vapor mass fraction, gas temperature and gas velocity are depicted in Figure 5.8. The overall agreement is satisfactory, particularly for mixture

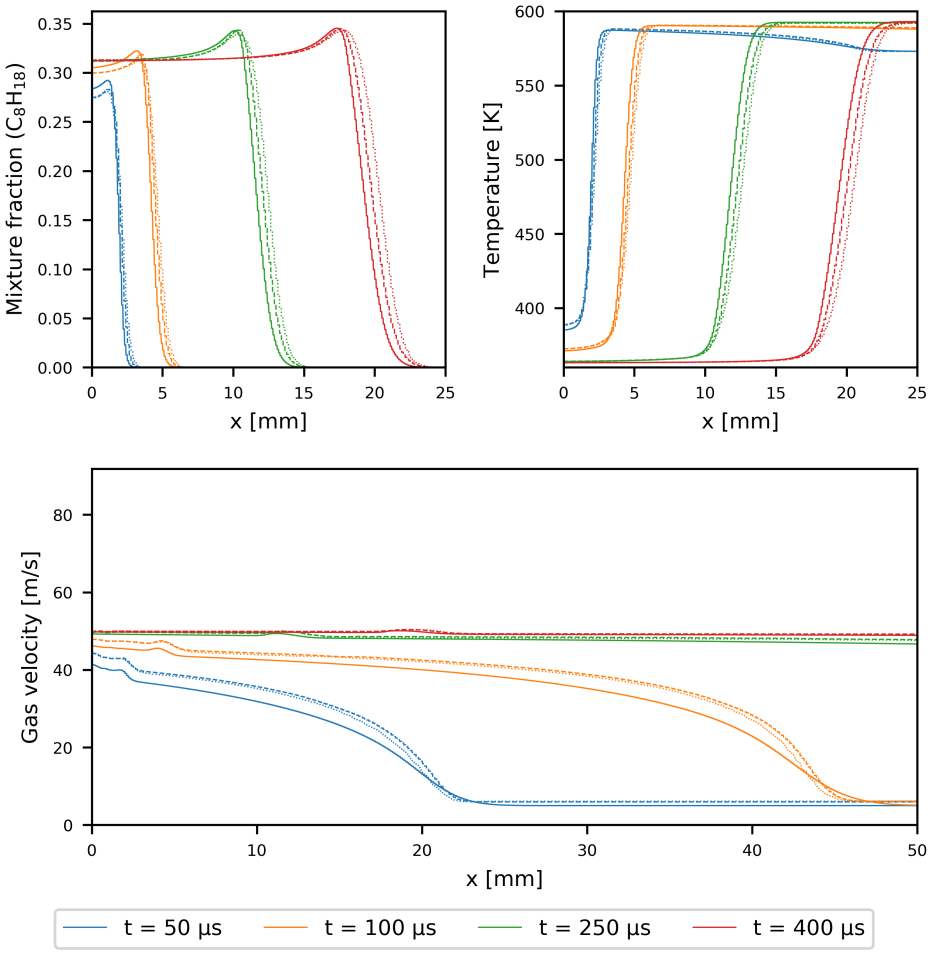

Figure 5.8: *Gas phase properties from EQMOM simulations compared to a LPT simulation. The solid lines represent the Lagrangian simulation, the dotted line EQMOM with a first-order advection scheme and the dashed line EQMOM with a second-order advection scheme.*

fraction and temperature. For the mixture fraction, this can be explained by the direct dependence of mass transfer on the internal coordinate. With regard to the temperature, the droplet heating under the given Spray G conditions up to a steady evaporation temperature occurs fast with the result that the size-dependence is negligible. The dependence of momentum transfer on particle size though is stronger, since the relaxation times are not as short. Therefore, the velocity field is noticably affected by the mean-velocity approach. Interestingly, the second-order advection has only a minor positive effect on accuracy in all cases. The relatively large deviation of all fields during the early

injection phase indicates that QBMM require some sort of special boundary treatment for spray modeling. Moreover, the transport of mean droplet temperatures is probably sufficient under typical conditions of evaporating sprays, whereas the droplet velocity components should be considered as additional internal coordinates in the PBE.

5.3 Secondary Atomization with QBMM

In this section, simulation results of secondary atomization with QBMM and the comparison with Lagrangian models are discussed. Investigations are carried out on zero-dimensional cases with constant gas properties. The model of Reitz and Diwakar, which was described in Section 4.4.2.1 and formulated for QBMM in Section 4.4.3, was employed as the atomization model. Additionally, a modified Lagrangian Reitz-Diwakar model was implemented, generating child parcels in each time step instead of applying the rate equation (Eq. 4.15). Therefore, the results of the modified Lagrangian model can serve as a reference solution for QBMM. It should be noted that this approach is not suitable for spray simulations due to prohibitive numerical costs.

For the isolated validation of both the bag breakup (*Case 1*) and the shear breakup (*Case 2*) regime, monodisperse populations were studied first. The conditions were chosen appropriately corresponding to the studied breakup regime. A summary of the population types, breakup modes, characteristic dimensionless quantities and the EQMOM setup for each test case is given in Table 5.3. For the polydisperse population, a Beta distribution was chosen. The PDF is defined as

$$\mathrm{Beta}(\xi;\alpha,\beta) = \frac{1}{\mathrm{B}(\alpha,\beta)}\xi^{\alpha-1}(1-\xi)^{\beta-1}, \tag{5.2}$$

where $B(\alpha,\beta)$ denotes the beta function. While the standard Lagrangian simulation was initialized by sampling 1000 particles from the given distribution, the simulation with the modified model was started with eight parcels located at the quadrature nodes of the distribution in order to ensure the accuracy of the initial moment set for the sake of comparability. The EQMOM calculation was initialized with the exact first $2N_\alpha$ moments from Eq. 5.2.

The moments up to fourth order computed in *Case 1* are shown in Figure 5.9. Naturally, the third moment remains constant due to the conservation of mass. No larger deviations can be identified. However, it is evident that the droplet population is hardly affected by atomization using the Reitz-Diwakar model under the studied conditions. Considering the zeroth moment, it becomes apparent that the total number of droplets is only multiplied by $\approx$1.25. This suggests that the Reitz-Diwakar model may not be suitable in the bag breakup regime. In this context, it is worth mentioning that the prioritization of shear breakup, when the conditions for both breakup modes are satisfied, considerably reduces the range of Weber and Reynolds numbers where bag breakup can occur.

Figure 5.10 illustrates the resulting moments in *Case 2*. The solution of the QBMM

Table 5.3: Summary of the test cases for secondary atomization

	Case 1	Case 2	Case 3
Droplet population	Monodisperse	Monodisperse	Beta(2, 5)
Breakup mode	Bag breakup	Shear breakup	Mixed
Weber number	13	192	0.5 - 305
Reynolds number	465	2005	6 - 3177
Ohnesorge number	0.02	0.02	0.02 - 0.38
	Beta KDF	Beta KDF	Beta KDF
EQMOM setup	$N_\alpha = 2$	$N_\alpha = 2$	$N_\alpha = 2$, $N_\alpha = 3$
	$N_{\alpha,\beta} = 10$	$N_{\alpha,\beta} = 10$	$N_{\alpha,\beta} = 10$

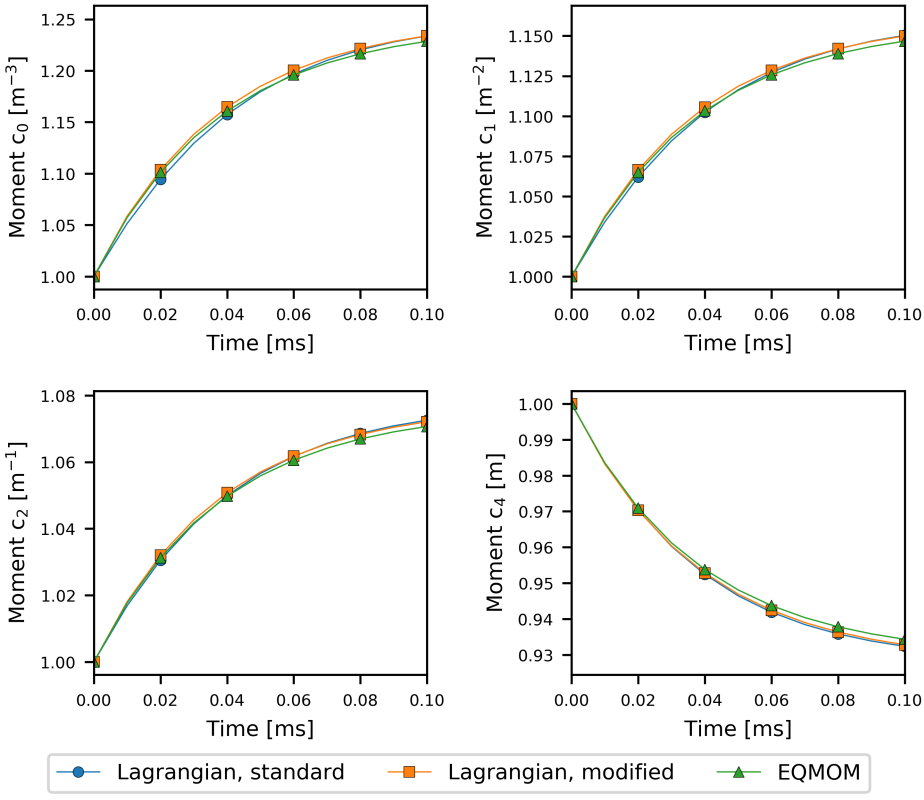

Figure 5.9: *Moments from secondary atomization simulations,* Case 1.

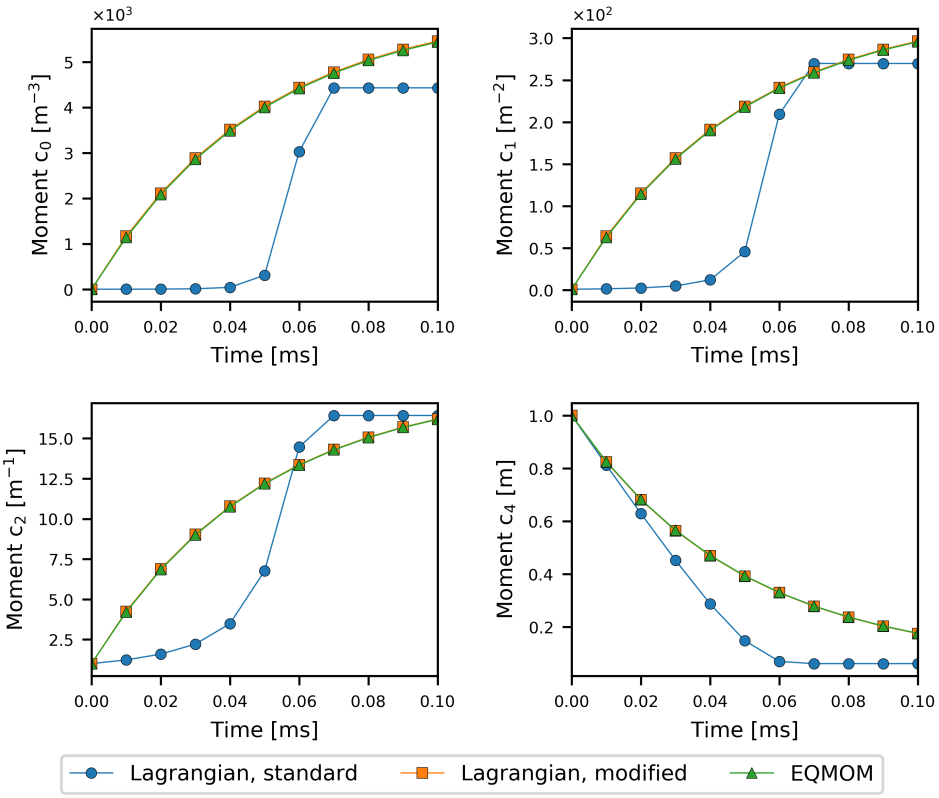

Figure 5.10: *Moments from secondary atomization simulations,* Case 2.

simulation agrees well with the Lagrangian reference solution with no visible difference. The virtually exact agreement is explicable by the Reitz-Diwakar model formulation: Since the fragment size in the shear breakup regime is only determined by the Weber and Reynolds number, the droplets of a monodisperse population can disintegrate into product droplets of only a single size. That is, at constant flow conditions the overall size distribution is merely the sum of two Dirac Delta functions located at the parent drop size and the fixed daughter drop size. Thus, the approximation of the NDF with $N_\alpha = 2$ first quadrature nodes is accurate. The standard Lagrangian model however deviates considerably, since no variance is introduced due to the diameter rate equation. In other words, a monodisperse system remains monodisperse despite the presence of fragmentation processes.

As discussed above, an accurate solution in case of a monodisperse population originates from the model formulation in combination with a two-node quadrature approximation. Figure 5.11 shows the results of *Case 3*, where the initial droplet population was polydisperse. In contrast to *Case 1* and *Case 2*, the results exhibit visible differences as

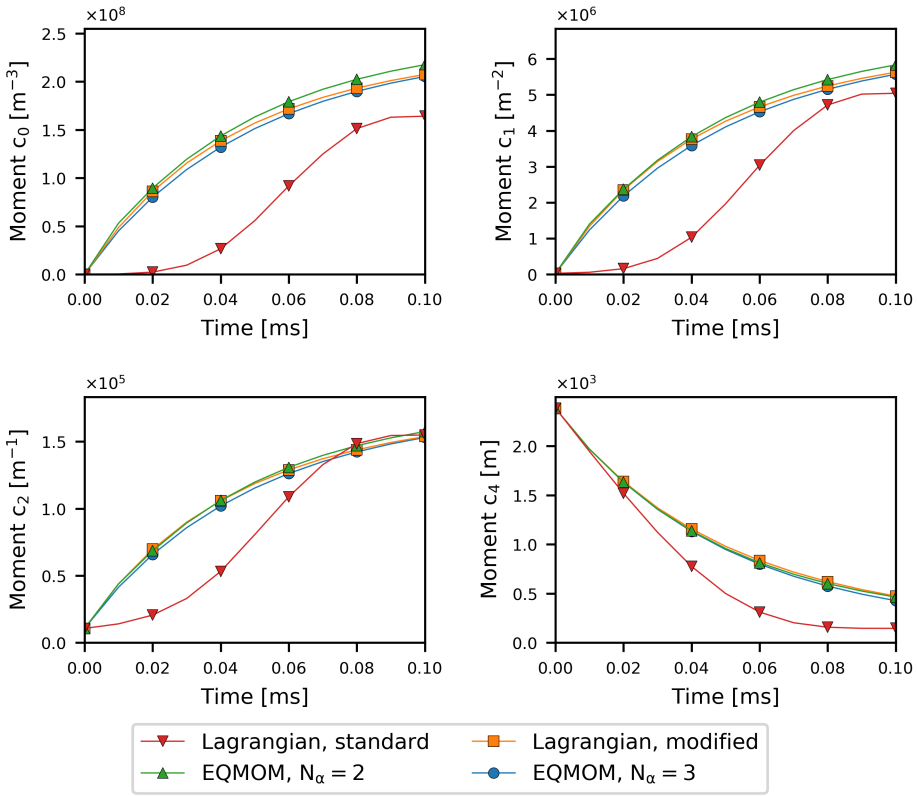

Figure 5.11: *Moments from secondary atomization simulations,* Case 3.

expected. Raising the number of first quadrature nodes to $N_\alpha = 3$ has only a minor effect on accuracy. The overall agreement with the reference solution is reasonable in both cases, but further investigation is necessary to evaluate the effects on the gas phase properties, e.g. mixture fraction by evaporation. Similar to the cases above, the Lagrangian standard model also exhibits significant deviations when the population is polydisperse. The terminal mean diameters agree with the modified Lagrangian model and EQMOM, which is not surprising considering the steady-state flow conditions. This is illustrated in Figure 5.12 in terms of the number-mean diameter $d_{10} = c_1/c_0$ and the Sauter mean diameter $d_{32} = c_3/c_2$ which is an important characteristic property in sprays.

To conclude, the results of simulations of secondary breakup show that the QBMM formulation gives the expected results compared with a Lagrangian reference solution. However, further studies need to be conducted to quantify the effects of small deviations on the droplet-gas interaction and mixture formation. Moreover, the derivation for multivariate PBEs is necessary to advance QBMM towards the application to sprays of practical relevance. A substantial advantage of the QBMM formulation over Lagrangian

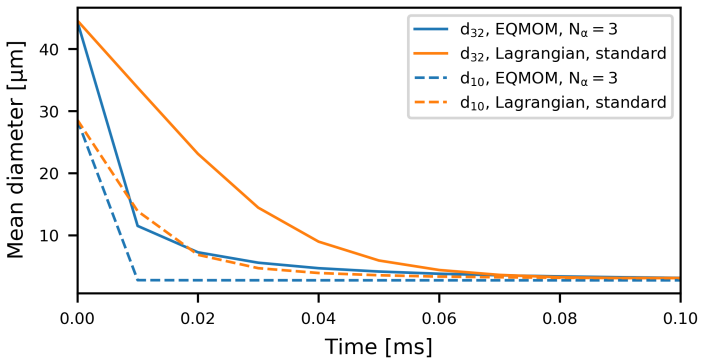

Figure 5.12: *Mean diameters from secondary atomization simulations,* Case 3.

models is that the daughter size distribution is not restricted by computational costs. That allows the development of more sophisticated models, which is also a subject of future research.

6 Conclusions and Future Work

The study of multiphase flows is of paramount importance to understand common physical phenomena occurring in nature and technology. Dispersed multiphase flows are a spcific type where one phase is present in the form of fine particles. A well-known technical application that highlights the significance of such flows is a spray, which refers to a system of fine liquid droplets, evolving in and interacting with a continuous gas phase. In propulsion systems involving the combustion of liquid fuels, the spray formation has significant effects on efficiency and the emission of pollutants. Besides theoretical analysis and experimental techniques, numerical modeling has gained increasing attention as a consequence of the rapidly increased availability of computational power over the past few decades. Numerical models can serve as a valuable tool to gain understanding of physical phenomena and predict their outcome. That knowledge can be utilezed to optimize spray systems. For that purpose however, predictive and computationally efficient models for dispersed multiphase flows are crucial.

The main objective of this thesis was the investigation of numerical modeling approaches for sprays. After providing the general mathematical description of dispersed multiphase systems in terms of the continuous phase and the dispersed phase, the focus was on representations of particulate systems, more precisely population balance equations and methods to approximate their solutions. Besides Lagrangian methods, a family of population balance models exploiting integral properties of local distributions, the so-called quadrature-based moment methods (QBMM), were a central subject of this thesis.

Moreover, physical aspects of sprays and their treatment with computational methods were discussed. In general, the physical processes taking place in a spray system can be identified as the internal nozzle flow potentially including cavitation, breakup of the continuous liquid jet exiting the nozzle (primary atomization), breakup of the formed strucures into smaller droplets (secondary atomization) and droplet vaporization. Here, a particular focus was on primary and secondary atomization. After a discussion of the mechanisms causing the different types of atomization, some computational models were presented, namely the one-dimensional turbulence (ODT) model and Lagrangian models for primary atomization as well as Lagrangian secondary breakup models, one of which was also formulated for the application with QBMM.

The described models were utilized in numerical studies of sprays as well as less complex configurations for the validation of QBMM-related models. First, an investigation of a full gasoline spray, namely the Engine Combustion Network's Spray G, was carried out. Using only standard Eulerian-Lagrangian methods, the simulation can serve as a reference for other methods. The same spray was studied employing the ODT primary breakup model in conjunction with a standard Lagrangian particle tracking. The simulation gave overall promising results but clearly revealed limitations of the ODT model with respect to transient jet development, which requires further modeling efforts.

Relatively simple flow configurations were studied with QBMM in order to validate the methods and advance towards more complex simulations. The first investigation that was part of this work was carried out on a droplet population in a one-dimensional flow field. The reference solution was obtained from a highly-resolved Lagrangian simulation. The overall agreement was satisfactory. However, the result suggest that special numerical methods must be applied to the spray inflow boundary, where high gradients are present. The results also indicated that more complex, higher-dimensional methods should be used to accurately capture momentum transfer from droplets to the gas. These are subjects of future studies.

The second numerical study with QBMM was concentrated on secondary atomization applied to a zero-dimensional setup. The reference solution was obtained from a computation using a modified Lagrangian model, which is not applicable to real spray systems due to prohibitive numerical costs. The solution was also compared to the Lagrangian standard model. The QBMM simulation matched the reference solution well. The comparison to the standard model highlighted advantages resulting from the fundamental difference between the Eulerian QBMM and Lagrangian approaches, especially the possibility of more physical models for fragment size distributions. The development of advanced secondary atomization models suited for QBMM is ongoing research.

References

[1] Amsden, A., O'Rourke, P., and Butler, T. "KIVA-II: A computer program for chemically reactive flows with sprays". 1989.

[2] Apte, S., Gorokhovski, M., and Moin, P. "LES of atomizing spray with stochastic modeling of secondary breakup". *International Journal of Multiphase Flow*, 29(9): 1503–1522, 2003.

[3] Ashurst, W. T. and Kerstein, A. R. "One-dimensional turbulence: Variable-density formulation and application to mixing layers". *Physics of Fluids*, 17(2):025107, 2005.

[4] Ashurst, W. T. and Kerstein, A. R. "Erratum:"One-dimensional turbulence: Variable-density formulation and application to mixing layers"[Phys. Fluids 17, 025107 (2005)]". *Physics of Fluids*, 21(11):119901, 2009.

[5] Batchelor, G. K. *An Introduction to Fluid Dynamics*. Cambridge Mathematical Library. Cambridge University Press, 2000.

[6] Baumgarten, C. *Mixture Formation in Internal Combustion Engines*. Heat and Mass Transfer. Springer Berlin Heidelberg, 2006.

[7] Beale, J. C. and Reitz, R. D. "Modeling spray atomization with the Kelvin-Helmholtz/Rayleigh-Taylor hybrid model". *Atomization and Sprays*, 9(6), 1999.

[8] Bird, R. B., Stewart, W. E., and Lightfoot, E. N. *Transport Phenomena*. John Wiley & Sons, 2007.

[9] Brodkey, R. S. *The Phenomena of Fluid Motions*. Addison-Wesley series in chemical engineering. Reading, Mass. cop. 1967, 1967.

[10] Cao, X.-K., Sun, Z.-G., Li, W.-F., Liu, H.-F., and Yu, Z.-H. "A new breakup regime of liquid drops identified in a continuous and uniform air jet flow". *Physics of Fluids*, 19(5):057103, 2007.

[11] Chesnel, J., Reveillon, J., Demoulin, F.-X., and Ménard, T. "Subgrid analysis of liquid jet atomization". *Atomization and Sprays*, 21(1):41–67, 2011.

[12] Chiu, S. N., Stoyan, D., Kendall, W. S., and Mecke, J. *Stochastic Geometry and its Applications*. John Wiley & Sons, 2013.

[13] Chou, W.-H. and Faeth, G. "Temporal properties of secondary drop breakup in the bag breakup regime". *International journal of multiphase flow*, 24(6):889–912, 1998.

[14] Chou, W.-H., Hsiang, L.-P., and Faeth, G. "Temporal properties of drop breakup in the shear breakup regime". *International Journal of Multiphase Flow*, 23(4): 651–669, 1997.

[15] Chou, W.-H., Hsiang, L., and Faeth, G. "Temporal variation of drop properties and formation rates during secondary breakup". In *31st Joint Propulsion Conference and Exhibit, San Diego July 10-12*, 1995.

[16] Dai, Z. and Faeth, G. "Temporal properties of secondary drop breakup in the multimode breakup regime". *International Journal of Multiphase Flow*, 27(2): 217–236, 2001.

[17] Desjardins, O., Moureau, V., and Pitsch, H. "An accurate conservative level set/ghost fluid method for simulating turbulent atomization". *Journal of Computational Physics*, 227(18):8395–8416, 2008.

[18] Dette, H. and Studden, W. *The Theory of Canonical Moments with Applications in Statistics, Probability, and Analysis*. Wiley Subscription Services, Inc., A Wiley Company, 1997.

[19] Eggers, J. "Nonlinear dynamics and breakup of free-surface flows". *Reviews of Modern Physics*, 69(3):865, 1997.

[20] Eggers, J. and Villermaux, E. "Physics of liquid jets". *Reports on Progress in Physics*, 71(3):036601, 2008.

[21] Engine Combustion Network. "Spray G: Mesh and Geometry". `https://ecn.sandia.gov/gasoline-spray-combustion/computational-method/mesh-and-geometry`, 2018.

[22] Ferziger, J. H. and Peric, M. *Computational Methods for Fluid Dynamics*. Springer-Verlag Berlin Heidelberg, 2002.

[23] Fox, R. O. "Quadrature-based moment methods for polydisperse multiphase flows". In *Stochastic Methods in Fluid Mechanics*, pages 87–136. Springer, 2014.

[24] Fox, R. O. and Marchisio, D. L. *Multiphase Reacting Flows: Modelling and Simulation*, volume no. 492. Springer, Wien;New York;, 2007.

[25] Gautschi, W. *Orthogonal Polynomials: Computation and Approximation*. Numerical mathematics and scientific computation. Oxford University Press, 2004.

[26] Gelfand, B. "Droplet breakup phenomena in flows with velocity lag". *Progress in Energy and Combustion Science*, 22(3):201–265, 1996.

[27] Golub, G. H. and Welsch, J. H. "Calculation of Gauss quadrature rules". *Mathematics of Computation*, 23:221–230, 1969.

[28] Gordon, R. G. "Error bounds in equilibrium statistical mechanics". *Journal of Mathematical Physics*, 9(5):655–663, 1968.

[29] Guildenbecher, D. R., Gao, J., Chen, J., and Sojka, P. E. "Characterization of drop aerodynamic fragmentation in the bag and sheet-thinning regimes by crossed-beam, two-view, digital in-line holography". *International Journal of Multiphase Flow*, 94: 107–122, 2017.

[30] Guildenbecher, D., López-Rivera, C., and Sojka, P. "Secondary atomization". *Experiments in Fluids*, 46(3):371–402, 2009.

[31] Helmholtz, H. "XLIII. On discontinuous movements of fluids". *The London, Edinburgh, and Dublin Philosophical Magazine and Journal of Science*, 36(244): 337–346, 1868.

[32] Herrmann, M. "The influence of density ratio on the primary atomization of a turbulent liquid jet in crossflow". *Proceedings of the Combustion Institute*, 33(2): 2079–2088, 2011.

[33] Hirt, C. and Nichols, B. "Volume of fluid (VOF) method for the dynamics of free boundaries". *Journal of Computational Physics*, 39(1):201–225, 1981.

[34] Hsiang, L.-P. and Faeth, G. M. "Near-limit drop deformation and secondary breakup". *International Journal of Multiphase Flow*, 18(5):635–652, 1992.

[35] Hsiang, L.-P. and Faeth, G. M. "Drop properties after secondary breakup". 19(5): 721–735, 1993.

[36] Hsiang, L.-P. and Faeth, G. "Drop deformation and breakup due to shock wave and steady disturbances". *International Journal of Multiphase Flow*, 21(4):545–560, 1995.

[37] Hubbard, G., Denny, V., and Mills, A. "Droplet evaporation: effects of transients and variable properties". *International Journal of Heat and Mass Transfer*, 18(9): 1003–1008, 1975.

[38] Huh, K. Y., Lee, E., and Koo, J. "Diesel spray atomization model considering nozzle exit turbulence conditions". *Atomization and Sprays*, 8(4), 1998.

[39] Issa, R. I. "Solution of the implicitly discretised fluid flow equations by operator-splitting". *Journal of Computational Physics*, 62(1):40–65, 1986.

[40] Jalaal, M. and Mehravaran, K. "Transient growth of droplet instabilities in a stream". *Physics of Fluids*, 26(1):012101, 2014.

[41] Joseph, D., Beavers, G., and Funada, T. "Rayleigh–Taylor instability of viscoelastic drops at high Weber numbers". *Journal of Fluid Mechanics*, 453:109–132, 2002.

[42] Kerstein, A. R. "One-dimensional turbulence: model formulation and application to homogeneous turbulence, shear flows, and buoyant stratified flows". *Journal of Fluid Mechanics*, 392:277–334, 1999.

[43] Kerstein, A. R., Ashurst, W. T., Wunsch, S., and Nilsen, V. "One-dimensional turbulence: vector formulation and application to free shear flows". *Journal of Fluid Mechanics*, 447:85–109, 2001.

[44] Krzeczkowski, S. A. "Measurement of liquid droplet disintegration mechanisms". *International Journal of Multiphase Flow*, 6(3):227–239, 1980.

[45] Kulkarni, V. and Sojka, P. "Bag breakup of low viscosity drops in the presence of a continuous air jet". *Physics of Fluids*, 26(7):072103, 2014.

[46] Kull, H.-J. "Theory of the Rayleigh-Taylor instability". *Physics Reports*, 206(5): 197–325, 1991.

[47] Lamb, H. *Hydrodynamics*. Cambridge University Press, 1993.

[48] Lebas, R., Menard, T., Beau, P., Berlemont, A., and Demoulin, F. "Numerical simulation of primary break-up and atomization: DNS and modelling study". *International Journal of Multiphase Flow*, 35(3):247–260, 2009.

[49] Liao, Y. and Lucas, D. "A literature review of theoretical models for drop and bubble breakup in turbulent dispersions". *Chemical Engineering Science*, 64(15): 3389 – 3406, 2009.

[50] Madadi-Kandjani, E. and Passalacqua, A. "An extended quadrature-based moment method with log-normal kernel density functions". *Chemical Engineering Science*, 131:323–339, 2015.

[51] Manin, J., Jung, Y., Skeen, S. A., Pickett, L. M., Parrish, S. E., and Markle, L. "Experimental characterization of DI gasoline injection processes". *SAE Technical Paper 2015-01-1894*.

[52] Marchisio, D. L. and Fox, R. O. *Computational Models for Polydisperse Particulate and Multiphase Systems*. Cambridge University Press, 2013.

[53] McGraw, R. "Correcting moment sequences for errors associated with advective transport". *Brookhaven National Laboratory, Upton, NY*, 2006.

[54] McGraw, R. "Description of aerosol dynamics by the quadrature method of moments". *Aerosol Science and Technology*, 27(2):255–265, 1997.

[55] Miles, J. W. "On the generation of surface waves by shear flows Part 3. Kelvin-Helmholtz instability". *Journal of Fluid Mechanics*, 6(4):583–598, 1959.

[56] Moukalled, F., Mangani, L., and Darwish, M. *The Finite Volume Method in Computational Fluid Dynamics: An Advanced Introduction with OpenFOAM® and Matlab*, volume 113. Springer International Publishing, 1st edition, 2016.

[57] Movaghar, A., Linne, M., Herrmann, M., Kerstein, A., and Oevermann, M. "Modeling and numerical study of primary breakup under diesel conditions". *International Journal of Multiphase Flow*, 98:110–119, 2018.

[58] Movaghar, A., Linne, M., Oevermann, M., Meiselbach, F., Schmidt, H., and Kerstein, A. R. "Numerical investigation of turbulent-jet primary breakup using one-dimensional turbulence". *International Journal of Multiphase Flow*, 89:241–254, 2017.

[59] Nicholls, J. "Stream and droplet breakup by shock waves". Technical report, NASA SP-194, 1972.

[60] Osher, S. and Sethian, J. A. "Fronts propagating with curvature-dependent speed: algorithms based on Hamilton-Jacobi formulations". *Journal of Computational Physics*, 79(1):12–49, 1988.

[61] Patterson, M. A. and Reitz, R. D. "Modeling the effects of fuel spray characteristics on diesel engine combustion and emission". *SAE Technical Paper 980131*, 1998.

[62] Pigou, M., Morchain, J., Fede, P., Penet, M.-I., and Laronze, G. "New developments of the Extended Quadrature Method of Moments to solve Population Balance Equations". *Journal of Computational Physics*, 365:243–268, 2018.

[63] Pilch, M. and Erdman, C. "Use of breakup time data and velocity history data to predict the maximum size of stable fragments for acceleration-induced breakup of a liquid drop". *International Journal of Multiphase Flow*, 13(6):741–757, 1987.

[64] Plateau, J. *Statique expérimentale et théorique des liquides soumis aux seules forces moléculaires*. Number v. 2 in Statique expérimentale et théorique des liquides soumis aux seules forces moléculaires. Gauthier-Villars, 1873.

[65] Poinsot, T. and Veynante, D. *Theoretical and Numerical Combustion*. RT Edwards, Inc., 2005.

[66] Pollack, M., Pütz, M., Marchisio, D. L., Oevermann, M., and Hasse, C. "Zero-flux approximations for multivariate quadrature-based moment methods". *Submitted to the Journal of Computational Physics*, 2019.

[67] Pope, S. B. *Turbulent Flows*. Cambridge University Press, 2000.

[68] Ramkrishna, D. *Population Balances: Theory and Applications to Particulate Systems in Engineering*. Academic Press, 2000.

[69] Ranz, W. and Marshall, W. "Evaporation from drops". *Chemical Engineering Progress*, 48(3):141–146, 1952.

[70] Rayleigh, Lord. "On the instability of jets". *Proceedings of the London mathematical society*, 1(1):4–13, 1878.

[71] Rayleigh, Lord. "Investigation of the character of the equilibrium of an incompressible heavy fluid of variable density". *Scientific Papers*, pages 200–207, 1900.

[72] Reitz, R. D. "Modeling atomization processes in high-pressure vaporizing sprays". *Atomisation and Spray Technology*, 3(4):309–337, 1987.

[73] Reitz, R. D. and Diwakar, R. "Effect of drop breakup on fuel sprays". *SAE Technical Paper 860469*, 1986.

[74] Reitz, R. D. and Diwakar, R. "Structure of high-pressure fuel sprays". *SAE Technical Paper 870598*, 1987.

[75] Ross, S. M. *Introduction to Probability Models*. Academic Press, 2014.

[76] Sack, R. and Donovan, A. "An algorithm for Gaussian quadrature given modified moments". *Numerische Mathematik*, 18(5):465–478, 1971.

[77] Sagaut, P. *Large Eddy Simulation for Incompressible Flows*. Springer Verlag, DE, 3 edition, 2006.

[78] Sallam, K., Dai, Z., and Faeth, G. "Liquid breakup at the surface of turbulent round liquid jets in still gases". *International Journal of Multiphase Flow*, 28(3): 427–449, 2002.

[79] Sazhin, S. "Advanced models of fuel droplet heating and evaporation". *Progress in Energy and Combustion Science*, 32(2):162–214, 2006.

[80] Sazhin, S. *Droplets and Sprays*. Springer, 2014.

[81] Sharp, D. H. "Overview of Rayleigh-taylor instability". Technical report, Los Alamos National Lab., NM (USA), 1983.

[82] Sirignano, W. *Fluid Dynamics and Transport of Droplets and Sprays*. Cambridge University Press, 2010.

[83] Su, T. F., Patterson, M. A., Reitz, R. D., and Farrell, P. V. "Experimental and numerical studies of high pressure multiple injection sprays". *SAE Technical Paper 960861*, 1996.

[84] Taylor, G. I. "The instability of liquid surfaces when accelerated in a direction perpendicular to their planes. I". *Proceedings of the Royal Society of London. Series A. Mathematical and Physical Sciences*, 201(1065):192–196, 1950.

[85] Theofanous, T. "Aerobreakup of Newtonian and viscoelastic liquids". *Annual Review of Fluid Mechanics*, 43:661–690, 2011.

[86] Theofanous, T. and Li, G. "On the physics of aerobreakup". *Physics of fluids*, 20 (5):052103, 2008.

[87] Theofanous, T., Mitkin, V., Ng, C., Chang, C., Deng, X., and Sushchikh, S. "The physics of aerobreakup. II. Viscous liquids". *Physics of Fluids*, 24(2):022104, 2012.

[88] Thomson, S. W. "XLVI. Hydrokinetic solutions and observations". *The London, Edinburgh, and Dublin Philosophical Magazine and Journal of Science*, 42(281): 362–377, 1871.

[89] Versteeg, H. K. and Malalasekera, W. *An Introduction to Computational Fluid Dynamics: The Finite Volume Method*. Pearson Education, 2007.

[90] Vikas, V., Wang, Z. J., Passalacqua, A., and Fox, R. O. "Realizable high-order finite-volume schemes for quadrature-based moment methods". *Journal of Computational Physics*, 230(13):5328–5352, 2011.

[91] Wendt, J., editor. *Computational Fluid Dynamics*. Springer Berlin Heidelberg, Berlin, Heidelberg, 2009.

[92] White, F. *Fluid Mechanics*. McGraw-Hill series in mechanical engineering. McGraw Hill, 2011.

[93] Wilcox, D. *Turbulence Modeling for CFD*. Number v. 1 in Turbulence Modeling for CFD. DCW Industries, 2006.

[94] Wilf, H. *Mathematics for the Physical Sciences*. John Wiley and Sons, 1962.

[95] Williams, F. "Spray Combustion and Atomization". *The Physics of Fluids*, 1(6): 541–545, 1958.

[96] Wright, D. L. "Numerical advection of moments of the particle size distribution in Eulerian models". *Journal of Aerosol Science*, 38(3):352–369, 2007.

[97] Wright, D. L., McGraw, R., and Rosner, D. E. "Bivariate extension of the quadrature method of moments for modeling simultaneous coagulation and sintering of particle populations". *Journal of Colloid and Interface Science*, 236(2):242–251, 2001.

[98] Wu, P. and Faeth, G. M. "Onset and end of drop formation along the surface of turbulent liquid jets in still gases". *Physics of Fluids*, 7(11):2915–2917, 1995.

[99] Yuan, C. and Fox, R. "Conditional quadrature method of moments for kinetic equations". *Journal of Computational Physics*, 230(22):8216–8246, 2011.

[100] Yuan, C., Laurent, F., and Fox, R. "An extended quadrature method of moments for population balance equations". *Journal of Aerosol Science*, 51(0):1–23, 2012.

[101] Yuan, C. *Quadrature-Based Moment Methods for Polydisperse Multiphase Flow Modeling*. PhD thesis, Iowa State University, 2013.

[102] Zhao, H., Liu, H.-F., Li, W.-F., and Xu, J.-L. "Morphological classification of low viscosity drop bag breakup in a continuous air jet stream". *Physics of Fluids*, 22 (11):114103, 2010.

[103] Zhao, H., Liu, H.-F., Xu, J.-L., Li, W.-F., and Lin, K.-F. "Temporal properties of secondary drop breakup in the bag-stamen breakup regime". *Physics of Fluids*, 25 (5):054102, 2013.